Scholars' Mine

Summer 2018

Quantifying on-orbit performance of CubeSat micropropulsion systems by observing orbital element variations

Bradyn William Morton

QUANTIFYING ON-ORBIT PERFORMANCE OF CUBESAT MICROPROPULSION

SYSTEMS BY OBSERVING ORBITAL ELEMENT VARIATIONS

by

BRADYN WILLIAM MORTON

A THESIS

Presented to the Graduate Faculty of the

MISSOURI UNIVERSITY OF SCIENCE AND TECHNOLOGY

In Partial Fulfillment of the Requirements for the Degree

MASTER OF SCIENCE

in

AEROSPACE ENGINEERING

2018

Approved by

Dr. Hank Pernicka Advisor
Dr. Kyle DeMars
Dr. Serhat Hosder

ABSTRACT

The Advanced Propulsion Experiment mission in development by the Missouri University of Science and Technology's satellite research team (M-SAT) is a technology demonstration mission of a multi-mode propulsion system. The true test of any satellite propulsion system is the on-orbit performance. The purpose of this research is to develop methods for quantifying the on-orbit performance of the multi-mode propulsion system. This performance can be determined by observing the small variations in the orbital element parameters and using a differential corrector with the Gauss Variation of Parameter equations. Furthermore, this research could be used to determine and quantify a propulsion system's performance on-orbit without *a priori* knowledge of the capabilities of the system. This is potentially useful in passively acquiring knowledge of non-cooperative spacecraft.

ACKNOWLEDGMENTS

TABLE OF CONTENTS

Page

LIST OF ILLUSTRATIONS

LIST OF TABLES

NOMENCLATURE

Symbol	Description
A	Acceleration
I_{sp}	Specific impulse
J_2	2nd zonal harmonic coefficient
R	Potential function due to perturbations
$R_\oplus$	Average Earth radius
Ω	Right ascension of the ascending node
α	Thrust vector offset angle from truth
β	Thrust vector offset clock angle
$\boldsymbol{F}$	Force
$\boldsymbol{F}_\tau$	Force due to thrust
$\boldsymbol{F}_p$	Force due to perturbations excluding thrust
$\boldsymbol{\Phi}$	Matrix of partial derivatives of the Gaussian variation of parameter equations with respect to the accelerations due to perturbations
$\boldsymbol{\Phi}'$	Matrix of partial derivatives of the Gaussian variation of parameter equations with respect to the force due to perturbations
$\boldsymbol{\kappa}_0$	True initial Keplerian states
$\boldsymbol{\kappa}_f$	True final Keplerian states
$\boldsymbol{\kappa}_k$	Keplerian states at some measurement k
$\boldsymbol{\tau}$	True thrust
$\boldsymbol{f}$	Acceleration due to all perturbations
$\boldsymbol{f}_\tau$	Acceleration due to thrust
$\boldsymbol{f}_p$	Acceleration due to perturbations excluding thrust
$\dot{\boldsymbol{\kappa}}$	Keplerian state rates
λ	Earth longitude

μ	Earth gravitational constant
ν	True anomaly
ω	Arguement of perigee
ϕ_{gc}	Earth latitude
$\sigma_{v,rms}$	Cartesian velocity root mean square standard deviation
$\sigma_{x,rms}$	Cartesian position root mean square standard deviation
θ	Argument of latitude
$\tilde{\kappa}_f$	Estimated final Keplerian states
$\tilde{\tau}$	Estimated thrust
$\tilde{\tau}^+$	Corrected thrust estimate
$\tilde{\tau}^-$	Prior thrust estimate
a	Semimajor axis
e	Eccentricity
h	Angular momentum
i	Inclination
m	Satellite mass
r	Orbital radius
r_a	Orbit apogee
r_p	Orbit perigee
t_k	Time at some measurement k

1. INTRODUCTION

1.1. BACKGROUND

Small satellites and CubeSats are becoming more popular, and with advancing technology are able to function on-orbit longer than earlier missions in this class of SmallSats. Perturbations can result in a satellite drifting out of its desired operational orbit, rendering it less effective. If such a case occurs, orbital maintenance is performed to return the satellite to the nominal orbit. This is done by performing propulsive maneuvers that counteract the perturbing forces that cause this drift. Small satellites and CubeSats therefore need small propulsion systems that can perform such maneuvers, allowing for the satellites to stay in operation longer.

New propulsion systems are actively being researched and designed specifically with CubeSats in mind.[1,2] These new propulsions systems can demonstrate their performance through ground-based testing in vacuum chambers but it is difficult to correlate the performance in spaceflight from ground testing due to difficulties replicating the vacuum and weightlessness of space on the ground. This is especially true with electric propulsion systems due to the fact that ion thrusters require a vacuum to operate efficiently.[3] Therefore tests must be performed on-orbit to accurately determine the efficiency and quantify the thrust capabilities of the system so that the technology readiness level (TRL) of such micropropulsion thrusters can be increased.

1.2. PURPOSE AND MOTIVATION

Small satellites generally have limited mass and volume allocations available for propulsions systems, and therefore generally cannot have large propellant tanks on-board. Optimizing the consumption of propellant is therefore a priority for orbit and attitude

changing maneuvers. It is therefore useful to formulate an effective on-orbit testing approach/platform by which the performance of micropropulsion systems can be accurately measured and assessed. This was the overall goal of this thesis study, defined by two specific objectives: (1) estimating the actual on-orbit thrust performance given orbit/attitude measurement data down-linked during the mission, and (2) identifying on-orbit maneuver options that provide large orbit/attitude changes relative to the propellant mass consumed.

Accelerometers are sensors that can be used to measure non-gravitational acceleration of a satellite in space, and are perhaps the "obvious" first-choice to measure thrust (directly). However, most are not sufficiently accurate to measure the low thrust of electric propulsion systems, due to the sensor errors/noise, and those that can are very expensive or too large for SmallSats. State estimation can estimate the spacecraft position and velocity given sensor data, but can diverge quickly for maneuvering spacecraft with a poor thrust estimate. Because lower thrust systems cannot be directly measured or generally determined by performing state estimation, one common method of thrust determination is to perform orbit determination before and after the maneuver. Assessing the change in the orbit allows for the change in velocity (ΔV) to be determined for the maneuver, and by extension the thrust.[4]

As an alternative, this research utilizes the state measurements of a satellite and its flight path during a maneuver. The initial state at the beginning of the maneuver is used along with a thrust "guess" to propagate an estimated flight path and the residual of the measured (actual) flight path and the estimated are then used to correct the thrust estimate. This is done iteratively until the estimated flight path closely matches the measured path. The force corresponding to the final estimated flight path is then a reasonably close representation of the true thrust generated by the propulsion system.

1.3. ADVANCED PROPULSION EXPERIMENT (APEX)

Small satellites generally have very low volume, power, and mass allocations to accommodate a propulsion system (also referred to as "SWaP," size, weight, and power). Therefore when a propulsion system is used a choice must usually be made between high-thrust/low specific impulse (chemical) or low-thrust/high specific impulse (electric). The Missouri University of Science and Technology's Satellite Research team is developing a technology demonstration mission known as the Advanced Propulsion Experiment (APEX), that hosts a new multi-mode micropropulsion system.[5]

The system is capable of performing both high-thrust/low impulse (chemical) and low-thrust/high impulse (electric) maneuvers using the same propellant, feed system, and nozzle hardware. This system requires approximately the same volume and mass as either an electric or chemical propulsion system and allows for both a chemical and electric propulsion operation providing flexibility in mission design and operation.

Due to the capabilities of both chemical and electric propulsion, the APEX mission is used as a case study for this research. The primary goal of this research is determining a method to accurately quantify the performance of this multi-mode propulsion system in both chemical and electric modes from on-orbit measurement data.

1.4. THESIS ORGANIZATION

First, the two-body and J_2 system dynamics are discussed, deriving the Gauss variational of parameter equations for each. The first objective involves deriving the analytic thrust estimation methods as well as implementing a differential corrector using the Gaussian variation of parameter equations. Then, the second objective, the maneuver options used to determine the optimal maneuver for thrust determination, is discussed. Sections 6 and 7 discuss the simulations created/used and the findings of the study.

2. SYSTEM DYNAMICS

2.1. TWO-BODY DYNAMICS

The Gauss variation of parameter (VOP) equations define the Keplerian orbital element rate-of-change due to perturbing forces acting on the satellite that are expressed in terms of the Local Vertical Local Horizontal (LVLH) reference frame. The LVLH frame is composed of $\hat{r}$, $\hat{\theta}$, and $\hat{h}$ as shown in Figure 2.1.
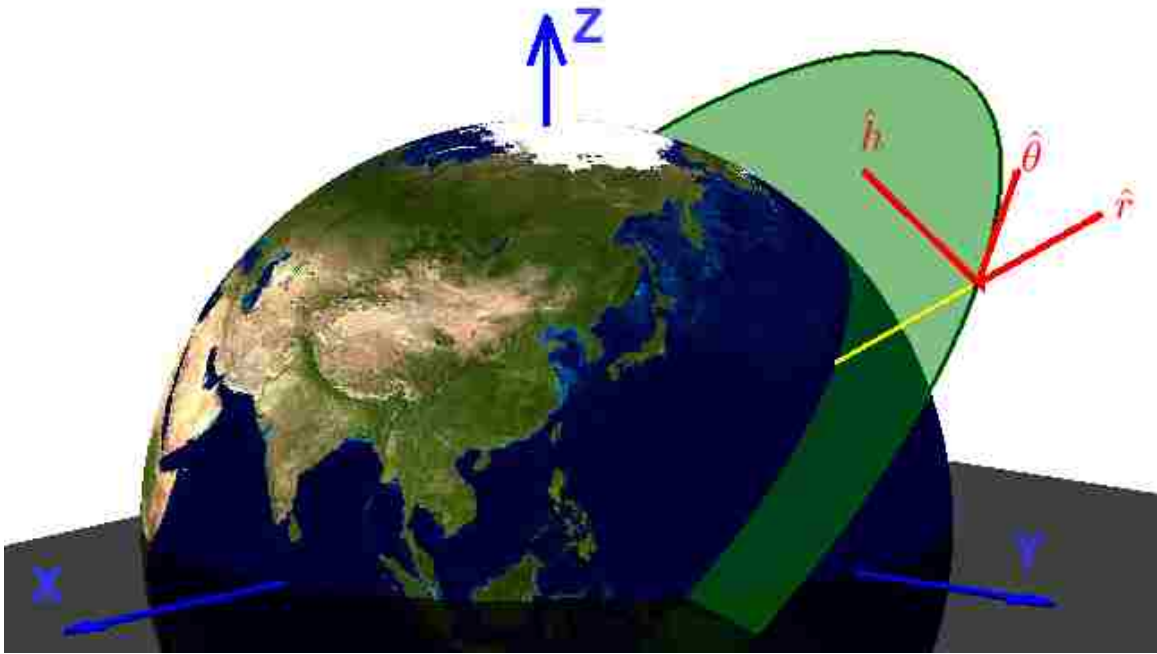
Figure 2.1. LVLH Reference Frame

The f_r and f_θ components are directed along the radial ($\hat{r}$) and local horizon ($\hat{\theta}$) directions respectively and the f_h component is normal to the orbit plane ($\hat{h}$) such that the cross product of $\hat{r}$ and $\hat{\theta}$ define $\hat{h}$ ($\hat{r} \times \hat{\theta} = \hat{h}$). The well-known Two-Body Gaussian VOP Equations are then[6]

$$\frac{da}{dt} = \frac{2a^2}{h}\left(e\sin(v)f_r + \frac{p}{r}f_\theta\right) \tag{2.1}$$

$$\frac{de}{dt} = \frac{1}{h}\left[p\sin(v)f_r + \Big((p+r)\cos(v) + re\Big)f_\theta\right] \tag{2.2}$$

$$\frac{di}{dt} = \frac{r\cos(\theta)}{h}f_h \tag{2.3}$$

$$\frac{d\Omega}{dt} = \frac{r\sin(\theta)}{h\sin(i)}f_h \tag{2.4}$$

$$\frac{d\omega}{dt} = \frac{1}{he}\left[-p\cos(v)f_r + (p+r)\sin(v)f_\theta\right] - \frac{r\cot(i)\sin(\theta)}{h}f_h \tag{2.5}$$

$$\frac{dv}{dt} = \frac{h}{r^2} + \frac{1}{he}\left[p\cos(v)f_r - (p+r)\sin(v)f_\theta\right] \tag{2.6}$$

$$\frac{d\theta}{dt} = \frac{h}{r^2} - \frac{r\cot(i)\sin(\theta)}{h}f_h \tag{2.7}$$

where the orbital radius, r, and angular momentum, h, are

$$r = \frac{a(1-e^2)}{1 + e\cos(v)} \quad \text{and} \quad h = \sqrt{\mu a(1-e^2)}$$

The full derivation can be found in Appendix A.

2.2. J_2 PERTURBATION DYNAMICS

Figure 2.2 shows the gravitational harmonics for $\ell = 2$ through 5 and $m = 0$.[6]
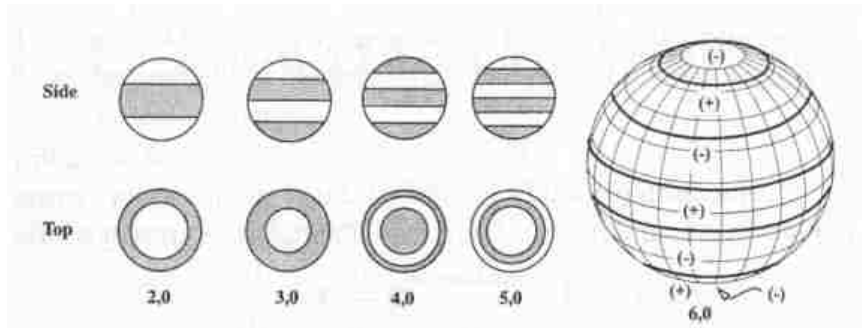
Figure 2.2. Gravitational Harmonics, $\ell = 2$ through 5, $m = 0$

Typically, a significant orbital perturbation for low Earth orbiting spacecraft are the Zonal Harmonics, especially J_2. The spherical harmonics disturbed potential function, R, is defined as[6]

$$R = -\frac{\mu}{r}\left[\sum_{\ell=2}^{\infty} J_\ell \left(\frac{R_\oplus}{r}\right)^\ell P_{\ell,0}\left[\sin\left(\phi_{gc}\right)\right] + ...\right.$$

$$\left.... + \sum_{\ell=2}^{\infty}\sum_{m=1}^{\ell} \left(\frac{R_\oplus}{r}\right)^\ell P_{\ell,m}\left[\sin\left(\phi_{gc}\right)\right]\left[C_{\ell,m}\cos\left(m\lambda\right) + S_{\ell,m}\sin\left(m\lambda\right)\right]\right]$$

where $R_\oplus$, is the average radius of the Earth, $C_{\ell,m}$ and $S_{\ell,m}$ are gravitational coefficients, J_ℓ are the zonal harmonic coefficients, ϕ_{gc} and λ are latitude and longitude of the satellite respectively, $P_{\ell,m}[\gamma]$ are the Legendre polynomials, and ℓ and m are the Legendre polynomial degree and order respectively; the Legendre polynomials for the first four zonal harmonics can be found in Appendix B. The potential function R can also be derived to include third body and other conservative forces resulting in higher fidelity VOP equations.

It is possible to determine the disturbing potential for J_2 only by defining $\ell = 2$, $m = 0$, and neglecting the tesseral and sectoral harmonics, resulting in

$$R = -\frac{\mu J_2}{r}\left(\frac{R_\oplus}{r}\right)^2 P_{2,0}\left[\sin\left(\phi_{gc}\right)\right]$$

The disturbing potential can be rewritten in a more useful form as

$$R = -\frac{\mu J_2}{r}\left(\frac{R_\oplus}{r}\right)^2 P_{2,0}\left[\sin\left(\phi_{gc}\right)\right] \qquad \text{where} \quad P_{2,0}[\gamma] = \frac{3}{2}\left(\gamma^2 - 1/3\right)$$

$$= -\frac{\mu J_2}{r}\left(\frac{R_\oplus}{r}\right)^2 \frac{3}{2}\left(\sin^2\left(\phi_{gc}\right) - \frac{1}{3}\right) \qquad \text{where} \quad \sin\phi_{gc} = \sin\left(i\right)\sin\left(\omega + v\right)$$

$$= -\frac{\mu J_2}{r}\left(\frac{R_\oplus}{r}\right)^2 \frac{3}{2}\left(\sin^2\left(i\right)\sin^2\left(\omega + v\right) - \frac{1}{3}\right)$$

$$= -\frac{3\mu J_2 R_\oplus^2}{2r^3}\left(\sin^2\left(i\right)\sin^2\left(\theta\right) - \frac{1}{3}\right) \qquad (2.8)$$

The perturbation acceleration components (f_r, f_θ, and f_h) can be determined and used in the Gaussian VOP equations if the disturbing potential R is known. Because R has now been defined for the J_2 perturbation only, by taking the vector gradient of R the J_2 acceleration components acting on the satellite in in terms of the LVLH reference frame can be found as[6]

$$f_{r,J_2} = \frac{\delta R}{\delta r} \qquad f_{\theta,J_2} = \frac{1}{r}\frac{\delta R}{\delta \theta} \qquad f_{h,J_2} = \frac{1}{r\sin(\theta)}\frac{\delta R}{\delta i} \qquad (2.9)$$

where the partials of Equation 2.8 are

$$\begin{aligned}
\frac{\delta R}{\delta r} &= \frac{\delta}{\delta r}\left[-\frac{3\mu J_2 R_\oplus^2}{2r^3}\left(\sin^2(i)\sin^2(\theta) - \frac{1}{3}\right)\right] \\
&= \frac{9\mu J_2 R_\oplus^2}{2r^4}\left(\sin^2(i)\sin^2(\theta) - \frac{1}{3}\right) \qquad (2.10)
\end{aligned}$$

$$\begin{aligned}
\frac{\delta R}{\delta \theta} &= \frac{\delta}{\delta \theta}\left[-\frac{3\mu J_2 R_\oplus^2}{2r^3}\left(\sin^2(i)\sin^2(\theta) - \frac{1}{3}\right)\right] \\
&= -\frac{3\mu J_2 R_\oplus^2}{r^3}\left(\sin^2(i)\sin(\theta)\cos(\theta)\right) \qquad (2.11)
\end{aligned}$$

$$\begin{aligned}
\frac{\delta R}{\delta i} &= \frac{\delta}{\delta i}\left[-\frac{3\mu J_2 R_\oplus^2}{2r^3}\left(\sin^2(i)\sin^2(\theta) - \frac{1}{3}\right)\right] \\
&= -\frac{3\mu J_2 R_\oplus^2}{r^3}\left(\sin^2(\theta)\sin(i)\cos(i)\right) \qquad (2.12)
\end{aligned}$$

Substituting Equations 2.10-2.12 into the perturbation acceleration equations, Equations 2.9 gives

$$f_{r,J_2} = \frac{9\mu J_2 R_\oplus^2}{2r^4}\left(\sin^2(i)\sin^2(\theta) - \frac{1}{3}\right)$$

$$f_{\theta,J_2} = -\frac{3\mu J_2 R_\oplus^2}{r^4} \left(\sin^2(i) \sin(\theta) \cos(\theta) \right)$$

$$f_{h,J_2} = -\frac{3\mu J_2 R_\oplus^2}{r^4} \left(\sin(\theta) \sin(i) \cos(i) \right)$$

the total perturbation acceleration components f_r, f_t, and f_h in the two-body VOP equations are given as

$$f_r = f_{r,\tau} + f_{r,J_2} \qquad f_\theta = f_{\theta,\tau} + f_{\theta,J_2} \qquad f_h = f_{h,\tau} + f_{h,J_2}$$

where $f_{r,\tau}$, $f_{\theta,\tau}$, and $f_{h,\tau}$ are the acceleration components from the applied thrust. This effectively reduces the two-body VOP equations into 2nd degree zonal harmonic VOP equations (J_2 VOP equations) given as

$$\frac{da}{dt} = \frac{2a^2}{h} \left[e \sin(v) \left\{ f_{r,\tau} + f_{r,J_2} \right\} + \frac{p}{r} \left\{ f_{\theta,\tau} + f_{\theta,J_2} \right\} \right] \tag{2.13}$$

$$\frac{de}{dt} = \frac{1}{h} \left[p \sin(v) \left\{ f_{r,\tau} + f_{r,J_2} \right\} + \left((p+r)\cos(v) + re \right) \left\{ f_{\theta,\tau} + f_{\theta,J_2} \right\} \right] \tag{2.14}$$

$$\frac{di}{dt} = \frac{r\cos(\theta)}{h} \left\{ f_{h,\tau} + f_{h,J_2} \right\} \tag{2.15}$$

$$\frac{d\Omega}{dt} = \frac{r\sin(\theta)}{h\sin(i)} \left\{ f_{h,\tau} + f_{h,J_2} \right\} \tag{2.16}$$

$$\frac{d\omega}{dt} = \frac{1}{he} \left(-p\cos(v) \left\{ f_{r,\tau} + f_{r,J_2} \right\} + (r+p)\sin(v) \left\{ f_{\theta,\tau} + f_{\theta,J_2} \right\} \right] - \ldots \tag{2.17}$$

$$\ldots - \frac{r\cot(i)\sin(\theta)}{h} \left\{ f_{h,\tau} + f_{h,J_2} \right\}$$

$$\frac{dv}{dt} = \frac{h}{r^2} + \frac{1}{he} \left(p\cos(v) \left\{ f_{r,\tau} + f_{r,J_2} \right\} - (r+p)\sin(v) \left\{ f_{\theta,\tau} + f_{\theta,J_2} \right\} \right) \tag{2.18}$$

$$\frac{d\theta}{dt} = \frac{h}{r^2} - \frac{r\cot(i)\sin(\theta)}{h} \left\{ f_{h,\tau} + f_{h,J_2} \right\} \tag{2.19}$$

3. ANALYTIC THRUST DETERMINATION (OBJECTIVE #1)

3.1. TWO-BODY THRUST DETERMINATION

The Gauss VOP equations can be integrated over short time spans given a few assumptions to determine the thrust force applied to the satellite. An example of this is shown for the thrust vector's $\hat{h}$-component using a RAAN (i.e., Ω) changing maneuver. The equations are coupled, but by making the assumption that the orbit is circular and that the inclination change is negligible, the $\dot{\Omega}$ equation can be decoupled from the others. Integrating this equation results in

$$
\begin{aligned}
\int_{\Omega_i}^{\Omega_f} d\Omega &= \int_{t_i}^{t_f} \frac{r f_{h,\tau} \sin(\theta)}{h \sin(i)} dt \\
&= \frac{r f_{h,\tau}}{h \sin(i)} \int_{t_i}^{t_f} \sin(\theta) dt \quad \text{where} \quad \frac{h}{r^2} dt = d\theta \\
&= \frac{r^3 f_{h,\tau}}{h^2 \sin(i)} \int_{\theta_i}^{\theta_f} \sin(\theta) d\theta \\
&= \frac{r^3 f_{h,\tau}}{h^2 \sin(i)} (-\cos(\theta)) \big|_{\theta_i}^{\theta_f} \\
\Delta\Omega_F &= \frac{r^3 f_{h,\tau}}{h^2 \sin(i)} \left(\cos(\theta_i) - \cos(\theta_f)\right)
\end{aligned}
\tag{3.1}
$$

where t_i and t_f are the maneuver start and finish times respectively and $f_{h,\tau}$ and $\Delta\Omega_F$ are the h component of thrust with respect to the LVLH reference frame and change in Ω due to thrust respectively. Rearranging to solve for thrust gives

$$f_{h,\tau} = \frac{F_h}{m} = \frac{\Delta\Omega_F h^2 \sin(i)}{r^3 \left(\cos(\theta_i) - \cos(\theta_f)\right)} \tag{3.2}$$

$$F_h = \frac{\Delta\Omega_F h^2 m \sin(i)}{r^3 \left(\cos(\theta_i) - \cos(\theta_f)\right)} \tag{3.3}$$

where m is the mass of APEX and n is the mean motion in rad/s.

3.2. J_2 THRUST DETERMINATION

By recognizing that the change in Ω could also be affected by perturbations (in addition to thrust), an improvement in the accuracy of the thrust estimation can be made by accounting for Earth's oblateness. Each effect can be estimated separately as

$$\Delta\Omega_{total} = \Delta\Omega_F + \Delta\Omega_{J2} \quad \Rightarrow \quad \Delta\Omega_F = \Delta\Omega_{total} - \Delta\Omega_{J2}$$

where $\Delta\Omega_{J2}$ is determined by analytically integrating $d\Omega/dt$ and $\Delta\Omega_{total}$ is the total Ω change occurring during the maneuver. The Ω rate due to the J_2 perturbation can be shown to be[6]

$$\begin{aligned}
\left(\frac{d\Omega}{dt}\right)_{J2} &= \frac{r\sin(\theta)}{h\sin(i)} f_{h,J_2} \\
&= \frac{r\sin(\theta)}{h\sin(i)} \left(-\frac{3\mu J_2 R_\oplus^2 \sin(\theta)\sin(i)\cos(i)}{r^4} \right) \\
&= -\frac{3\mu J_2 R_\oplus^2 \sin^2(\theta)\cos(i)}{hr^3}
\end{aligned}$$

Adding this equation to the Gaussian Two-body VOP equations results in

$$\dot{\Omega} = \frac{r\sin(\theta)}{h\sin(i)} f_{h,\tau} + \left(\frac{d\Omega}{dt}\right)_{J2}$$

and taking the integral of the J_2 portion assuming that n, a, e, i, and r are constant through-

out the maneuver results in

$$
\begin{aligned}
\int_0^t d\Omega &= \frac{-3\mu J_2 R_\oplus^2 \cos(i)}{hr^3} \int_0^t \sin^2(\theta)dt \qquad \text{where} \qquad \dot{\theta}dt = \frac{h}{r^2}dt = d\theta \\
&= \frac{-3\mu J_2 R_\oplus^2 \cos(i)}{h^2 r} \int_{\theta_i}^{\theta_f} \sin^2(\theta)d\theta \\
&= \frac{-3\mu J_2 R_\oplus^2 \cos(i)}{2h^2 r} \left[\theta - \sin(\theta)\cos(\theta) \right]_{\theta_i}^{\theta_f} \\
&= \frac{-3\mu J_2 R_\oplus^2 \cos(i)}{2h^2 r} \left[\{\theta_f - \theta_i\} - \{\sin(\theta_f)\cos(\theta_f) - \sin(\theta_i)\cos(\theta_i)\} \right]
\end{aligned}
$$

Adding this to the two-body $\Delta\Omega_F$ equation gives

$$
\begin{aligned}
\Delta\Omega_{total} &= \Delta\Omega_F + \Delta\Omega_{J2} \\
&= \frac{r^3}{h^2 \sin(i)} \left[\cos(\theta_i) - \cos(\theta_f) \right] f_{h,\tau} - \ldots \\
&\quad \ldots \frac{-3\mu J_2 R_\oplus^2 \cos(i)}{2h^2 r} \left[\{\theta_f - \theta_i\} - \{\sin(\theta_f)\cos(\theta_f) - \sin(\theta_i)\cos(\theta_i)\} \right]
\end{aligned}
$$

and after rearranging the thrust can be shown to be

$$
F_h = \left[\Delta\Omega_{total} + \frac{3\mu J_2 R_\oplus^2 \cos(i)}{2h^2 r} \left(\{\theta_f - \theta_i\} - \{\sin(\theta_f)\cos(\theta_f) - \sin(\theta_i)\cos(\theta_i)\} \right) \right] \times \ldots
$$

$$
\ldots \times \frac{mh^2 \sin(i)}{r^3 \left[\cos(\theta_i) - \cos(\theta_f) \right]}
$$

This can be expanded to higher order zonal harmonics to increase the accuracy and can

provide a good initial guess for numerical methods and filters for orbit determination and

thrust validation.

4. NUMERICAL THRUST DETERMINATION WITH A DIFFERENTIAL CORRECTOR

To numerically determine thrust a differential corrector was used. Differential correctors are generally used with a set of equations to determine the value of an input variable to achieve a desired outcome or drive some cost function to zero.[7] This is done iteratively by using a linear approximation of how a needed change in the outcome changes the input variable.[8]

In this section, it is assumed that multiple GPS measurements were taken (simulated in this thesis study) at the beginning and end of some maneuver that spans time Δt (t_0 to t_f) and that these position and velocity measurements were transformed into Keplerian orbital elements. These true (uncorrupted) Keplerian elements were used as the measured orbital elements (the initial/final states) for this section. The goal is then to determine the thrust force applied from t_0 to t_f from the measured (true) Keplerian element change.

In general, the following method can be performed over any time scale. Let t_k be an arbitrary point in time during the maneuver with an associated Cartesian state measurement ($\boldsymbol{x}_k$). Using the initial measured Keplerian state ($\boldsymbol{\kappa}_0$, converted from $\boldsymbol{x}_0$) and an initial guess/estimate of some force (thrust, drag, solar radiation pressure, etc.) acting on the satellite, an estimated state ($\tilde{\boldsymbol{\kappa}}_k$) at time t_k can be determined by numerically propagating $\boldsymbol{\kappa}_0$ from t_0 to t_k indicated by the red line in Figure 4.1. The difference between the measured final state ($\boldsymbol{\kappa}_k$ in green) and the estimated final state ($\tilde{\boldsymbol{\kappa}}_k$ in red), as shown in Figure 4.1, is then the residual state ($\Delta\boldsymbol{\kappa}$).

The goal is to drive the residual to zero, resulting in the estimated force being approximately equal to the actual force applied to obtain the final measured state. When the residual state is not equal to zero, the force guess requires correcting so that the estimated orbital trajectory more closely matches the measured. This is done with a differential corrector utilizing the Gaussian VOP equations.
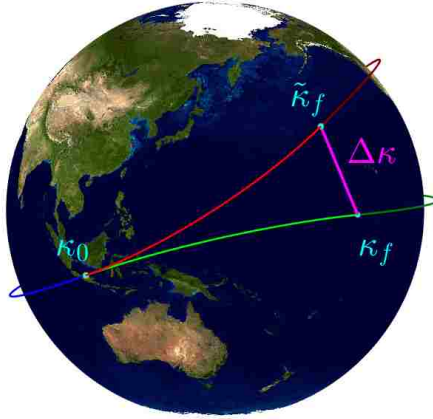
Figure 4.1. Residual Resulting from Inaccurate Thrust Estimate

4.1. DERIVATION OF THRUST DETERMINATION EQUATIONS

The differential corrector uses the difference between a measured state at some point in time (t_k) and the propagated state estimate at the same time to determine the change in the thrust vector estimate that reduces the final state residual until some small tolerance is met. The Gaussian VOP equations (2.1-2.7) can be approximated over a small Δt as a set of coupled equations as

$$
\begin{bmatrix} \Delta a \\ \Delta e \\ \Delta i \\ \Delta \omega \\ \Delta \Omega \\ \Delta \nu \end{bmatrix} = \boldsymbol{\Phi} \begin{bmatrix} f_r \\ f_\theta \\ f_h \end{bmatrix} \Delta t + \begin{bmatrix} 0 \\ 0 \\ 0 \\ 0 \\ 0 \\ \frac{h}{r^2} \end{bmatrix} \Delta t \quad \Rightarrow \quad \Delta \boldsymbol{\kappa} = \boldsymbol{\Phi} \boldsymbol{f} \Delta t + \boldsymbol{n} \Delta t \tag{4.1}
$$

where $\boldsymbol{\Phi}$ is the matrix partial derivatives of the Gaussian VOP equations with respect to $\boldsymbol{f}$, or

$$
\boldsymbol{\Phi} = \frac{\partial \dot{\boldsymbol{\kappa}}}{\partial \boldsymbol{f}} \tag{4.2}
$$

where the state vector $\boldsymbol{\kappa}$ is defined as a vector of the Keplerian orbital elements. The Gaussian VOP equations and the approximation in Equation 4.1 give the Keplerian orbital element rates as a function of the accelerations f_r, f_θ, and f_h. By varying these accelerations acting on the satellite, the estimated orbital elements can more closely fit the state measurements. The perturbing acceleration components are defined as

$$f_r = f_{r,\tau} + f_{r,p} \quad \text{where} \quad f_{r,\tau} = \frac{\tau_r}{m} \tag{4.3}$$

$$f_\theta = f_{\theta,\tau} + f_{\theta,p} \quad \text{where} \quad f_{\theta,\tau} = \frac{\tau_\theta}{m} \tag{4.4}$$

$$f_h = f_{h,\tau} + f_{h,p} \quad \text{where} \quad f_{h,\tau} = \frac{\tau_h}{m} \tag{4.5}$$

where τ_r, τ_θ, and τ_h are the thrust components expressed in terms of the LVLH frame, $f_{r,p}$, $f_{\theta,p}$, and $f_{h,p}$ are the acceleration components due to perturbations (excluding thrust), and m is the mass of the satellite. Because the larger perturbations are well known, and high fidelity dynamic models accurately quantify these resulting accelerations, the only acceleration that is unknown (and sought) is the acceleration due to thrust ($\boldsymbol{f}_\tau$).

A complication is that Equation 4.1 is defined as the change in orbital elements, not thrust, so it must be solved for $\boldsymbol{f}$, or more specifically $\boldsymbol{f}_\tau$ (the acceleration due to thrust). So to calculate the thrust ($\boldsymbol{\tau} = m\boldsymbol{f}_\tau$), the matrix $\boldsymbol{\Phi}$ and vector $\boldsymbol{n}$ need to be determined throughout the time interval Δt. The matrix $\boldsymbol{\Phi}$, is found by recognizing how the change in the applied force acceleration ($\boldsymbol{f}$) affects the orbital elements. While Equation 4.1 is reasonably accurate over small time steps, it breaks down over long periods of time. Reverting back to the continuous form of the Gaussian VOP equations (Equations 2.1 - 2.6), the osculating (instantaneous) rate change of the orbital elements are defined as

$$\dot{\boldsymbol{\kappa}}(t) = \boldsymbol{\Phi}(t)\boldsymbol{f}(t) + \boldsymbol{n}(t) \tag{4.6}$$

which does not explicitly define how the orbital elements themselves change over a finite thrust time interval. If the Keplerian elements are known at some initial time t_0, then the future elements at time t_k can be determined as

$$
\begin{aligned}
\boldsymbol{\kappa}_k &= \boldsymbol{\kappa}_0 + \int_{t_0}^{t_k} \dot{\boldsymbol{\kappa}}(t)\, dt \\
&= \boldsymbol{\kappa}_0 + \int_{t_0}^{t_k} \left[\boldsymbol{\Phi}(t) \boldsymbol{f}(t) + \boldsymbol{n}(t) \right] dt
\end{aligned}
\tag{4.7}
$$

where $\boldsymbol{\kappa}_k$ is a vector of the orbital element state and t_0 is generally defined as $t_0 = 0$. Equation 4.7 is written in terms of acceleration ($\boldsymbol{f}$) and not force ($\boldsymbol{F}$), therefore let $\boldsymbol{\Phi}'$ be defined as the Jacobian matrix of the Gaussian VOP equations with respect to the force applied to the satellite ($\boldsymbol{F}$)

$$
\boldsymbol{\Phi}' = \frac{\partial \dot{\boldsymbol{\kappa}}}{\partial \boldsymbol{F}}
\tag{4.8}
$$

as with acceleration, $\boldsymbol{F}$ can be split into the force due to thrust ($\boldsymbol{\tau}$) and the forces due to other perturbations ($\boldsymbol{F}_p$). Remembering

$$
\boldsymbol{f} = \begin{bmatrix} f_r \\ f_\theta \\ f_h \end{bmatrix} = \begin{bmatrix} \frac{F_r}{m} \\ \frac{F_\theta}{m} \\ \frac{F_h}{m} \end{bmatrix}
$$

$$
\Rightarrow \quad \boldsymbol{F} = \begin{bmatrix} \tau_r + F_{r,p} \\ \tau_\theta + F_{\theta,p} \\ \tau_h + F_{h,p} \end{bmatrix} = \begin{bmatrix} m f_r \\ m f_\theta \\ m f_h \end{bmatrix}
$$

$\boldsymbol{\Phi}'$ maps $\boldsymbol{F}$ (the total applied force) to $\dot{\boldsymbol{\kappa}}$, and changes Equation 4.7 to

$$
\boldsymbol{\kappa}_k = \boldsymbol{\kappa}_0 + \int_{t_0}^{t_k} \left[\boldsymbol{\Phi}'(t) \boldsymbol{F}(t) + \boldsymbol{n}(t) \right] dt
\tag{4.9}
$$

$\mathbf{\Phi}'$ is then populated according to Equation 4.8

$$\mathbf{\Phi}' = \begin{bmatrix} \frac{\partial \dot{a}}{\partial F_r} & \frac{\partial \dot{a}}{\partial F_\theta} & \frac{\partial \dot{a}}{\partial F_h} \\[2mm] \frac{\partial \dot{e}}{\partial F_r} & \frac{\partial \dot{e}}{\partial F_\theta} & \frac{\partial \dot{e}}{\partial F_h} \\[2mm] \frac{\partial \dot{i}}{\partial F_r} & \frac{\partial \dot{i}}{\partial F_\theta} & \frac{\partial \dot{i}}{\partial F_h} \\[2mm] \frac{\partial \dot{\omega}}{\partial F_r} & \frac{\partial \dot{\omega}}{\partial F_\theta} & \frac{\partial \dot{\omega}}{\partial F_h} \\[2mm] \frac{\partial \dot{\Omega}}{\partial F_r} & \frac{\partial \dot{\Omega}}{\partial F_\theta} & \frac{\partial \dot{\Omega}}{\partial F_h} \\[2mm] \frac{\partial \dot{\nu}}{\partial F_r} & \frac{\partial \dot{\nu}}{\partial F_\theta} & \frac{\partial \dot{\nu}}{\partial F_h} \end{bmatrix}$$

The matrix $\mathbf{\Phi}'$ then approximates how changes in F_r, F_θ, and F_h will change the orbital element rates over the Δt time interval. The partials defining $\mathbf{\Phi}'$ are

$$\frac{\partial \dot{a}}{\partial F_r} = \frac{2a^2 e \sin(\nu)}{hm} \qquad \frac{\partial \dot{a}}{\partial F_\theta} = \frac{p}{rm} \qquad \frac{\partial \dot{a}}{\partial F_h} = 0$$

$$\frac{\partial \dot{e}}{\partial F_r} = \frac{p \sin(\nu)}{hm} \qquad \frac{\partial \dot{e}}{\partial F_\theta} = \frac{(p+r)\cos(\nu) + re}{hm} \qquad \frac{\partial \dot{e}}{\partial F_h} = 0$$

$$\frac{\partial \dot{i}}{\partial F_r} = 0 \qquad \frac{\partial \dot{i}}{\partial F_\theta} = 0 \qquad \frac{\partial \dot{i}}{\partial F_h} = \frac{r \cos(\theta)}{hm}$$

$$\frac{\partial \dot{\omega}}{\partial F_r} = \frac{-p \cos(\nu)}{hem} \qquad \frac{\partial \dot{\omega}}{\partial F_\theta} = \frac{(p+r)\sin(\nu)}{hem} \qquad \frac{\partial \dot{\omega}}{\partial F_h} = \frac{-r \cos(i) \sin(\theta)}{hm \sin(i)}$$

$$\frac{\partial \dot{\Omega}}{\partial F_r} = 0 \qquad \frac{\partial \dot{\Omega}}{\partial F_\theta} = 0 \qquad \frac{\partial \dot{\Omega}}{\partial F_h} = \frac{r \sin(\theta)}{hm \sin(i)}$$

$$\frac{\partial \dot{\nu}}{\partial F_r} = \frac{p \cos(\nu)}{hem} \qquad \frac{\partial \dot{\nu}}{\partial F_\theta} = \frac{-(p+r)\sin(\nu)}{hem} \qquad \frac{\partial \dot{\nu}}{\partial F_h} = 0$$

So $\mathbf{\Phi}'$ is then given as

$$\mathbf{\Phi}' = \begin{bmatrix} \frac{2a^2 e \sin(\nu)}{hm} & \frac{2a^2 p}{hrm} & 0 \\[3mm] \frac{p \sin(\nu)}{hm} & \frac{(p+r)\cos(\nu)+re}{hm} & 0 \\[3mm] 0 & 0 & \frac{r \cos(\theta)}{hm} \\[3mm] \frac{-p \cos(\nu)}{hem} & \frac{(p+r)\sin(\nu)}{hem} & \frac{-r \cos(i) \sin(\theta)}{hm \sin(i)} \\[3mm] 0 & 0 & \frac{r \sin(\theta)}{hm \sin(i)} \\[3mm] \frac{p \cos(\nu)}{hem} & \frac{-(p+r)\sin(\nu)}{hem} & 0 \end{bmatrix} \qquad (4.10)$$

Remembering that κ_0 is a known initial condition, and not a function of F, the change in the orbital elements with respect to changes in thrust becomes

$$
\begin{aligned}
\frac{\partial \kappa_k}{\partial F} &= \frac{\partial}{\partial F} \left(\kappa_0 + \int_{t_0}^{t_k} \left[\Phi'(t)F + n(t) \right] \, dt \right) \\
&= \int_{t_0}^{t_k} \frac{\partial}{\partial F} \left(\Phi'(t)F \right) dt + \int_{t_0}^{t_k} \underbrace{\frac{\partial}{\partial F} \left(n(t) \right)}_{\approx 0} dt \\
&= \int_{t_0}^{t_k} \Phi'(t) \, dt
\end{aligned}
\tag{4.11}
$$

the partial of $n(t)$ with respect to F is negligible due to the assumption, that low thrust will have a very small affect on orbit angular rate $\dot{\theta}$, therefore

$$
n = \begin{bmatrix} 0 & 0 & 0 & 0 & 0 & \frac{h}{r^2} \end{bmatrix}^T
$$

$$
\Rightarrow \quad \frac{h}{r^2} = \frac{\sqrt{\mu}(1 + e\cos(v))}{a^{3/2}(1 - e^2)^{3/2}} \approx \frac{\sqrt{\mu}}{a^{3/2}} \quad \text{where} \quad \begin{aligned} &\mu = 398600 \text{ km}^3/\text{s}^2 \\ &a > 6378.14 \text{ km} \end{aligned}
$$

$$
\Rightarrow \quad \frac{h}{r^2} \ll 1
$$

Φ' is a matrix populated with Keplerian elements (κ), and therefore is dependent upon time or $\Phi' = \Phi'(t)$ as shown in Equation 4.10. Therefore, to determine Φ' over a time interval Δt, a thrust guess ($\tilde{\tau}$) is required. This results in an estimated state ($\tilde{\kappa}_k$) at time t_k, given as

$$
\begin{aligned}
\tilde{\kappa}_k &= \kappa_0 + \int_{t_0}^{t_k} \left[\Phi'(t)\tilde{F}(t) + \tilde{n}(t) \right] dt \\
&= \kappa_0 + \int_{t_0}^{t_k} \left[\Phi'(t) \left[\tilde{\tau}(t) + \tilde{F}_p(t) \right] + \tilde{n}(t) \right] dt \\
&= \kappa_0 + \int_{t_0}^{t_k} \left[\Phi'(t)\tilde{\tau}(t) + \Phi'(t)\tilde{F}_p(t) + \tilde{n}(t) \right] dt \\
&= \kappa_0 + \int_{t_0}^{t_k} \left[\Phi'(t)\tilde{\tau}(t) + \dot{\tilde{\kappa}}_p(t) + \tilde{n}(t) \right] dt
\end{aligned}
\tag{4.12}
$$

where $\dot{\boldsymbol{\kappa}}_p(t)$ is the orbital element rate due to perturbations. Equation 4.12 describes the initial state ($\boldsymbol{\kappa}_0$) being propagated with the thrust guess ($\tilde{\boldsymbol{\tau}}$) for some time ($t_k$) to determine an estimated final state $\tilde{\boldsymbol{\kappa}}_k$. Subtracting the measured (truth) state ($\boldsymbol{\kappa}_k$) and estimated state ($\tilde{\boldsymbol{\kappa}}_k$) at t_k then results in

$$
\begin{aligned}
\Delta\boldsymbol{\kappa}_k &= \boldsymbol{\kappa}_k - \tilde{\boldsymbol{\kappa}}_k \\
&= \left[\boldsymbol{\kappa}_0 + \int_{t_0}^{t_k} \left(\boldsymbol{\Phi}'(t)\boldsymbol{\tau}(t) + \dot{\boldsymbol{\kappa}}_p(t) + \boldsymbol{n}(t) \right) dt \right] - \dots \\
&\quad \dots - \left[\boldsymbol{\kappa}_0 + \int_{t_0}^{t_k} \left(\boldsymbol{\Phi}'(t)\tilde{\boldsymbol{\tau}}(t) + \dot{\tilde{\boldsymbol{\kappa}}}_p(t) + \tilde{\boldsymbol{n}}(t) \right) dt \right]
\end{aligned}
\tag{4.13}
$$

where $\boldsymbol{\tau}$ is the true (unknown) thrust. In Equation 4.11 the partial of $\boldsymbol{n}$ with respect to $\boldsymbol{F}$ is assumed to be approximately zero, therefore, the partial of $\boldsymbol{n}$ with respect to $\boldsymbol{\tau}$ may also be approximately zero resulting in

$$
\boldsymbol{n}(t) - \tilde{\boldsymbol{n}}(t) \approx 0
$$

this can also be shown for the rates due to perturbations (excluding thrust)

$$
\frac{\partial \dot{\boldsymbol{\kappa}}_p}{\partial \boldsymbol{\tau}} \approx 0 \quad \Rightarrow \quad \dot{\boldsymbol{\kappa}}_p(t) - \dot{\tilde{\boldsymbol{\kappa}}}_p(t) \approx 0
$$

then simplifying Equation 4.13 results in

$$
\begin{aligned}
\Delta\boldsymbol{\kappa}_k &= \int_{t_0}^{t_k} \boldsymbol{\Phi}'(t)\boldsymbol{\tau}(t) \, dt - \int_{t_0}^{t_k} \boldsymbol{\Phi}'(t)\tilde{\boldsymbol{\tau}}(t) \, dt \\
&= \int_{t_0}^{t_k} \boldsymbol{\Phi}'(t)\Delta\boldsymbol{\tau}(t) \, dt
\end{aligned}
\tag{4.14}
$$

The only step now is to solve Equation 4.14 for $\Delta\boldsymbol{\tau}$. This will give an approximation for how the thrust guess should be updated to bring it closer to the truth.

4.2. CONSTANT THRUST VECTOR

If it is assumed the thrust vector is constant throughout the entire maneuver with respect to the LVLH reference frame, then the thrust vector can be removed from the integral and Equation 4.14 becomes

$$\Delta\boldsymbol{\kappa}_k = \left[\int_{t_0}^{t_f} \boldsymbol{\Phi}'(t)\, dt\right]\Delta\boldsymbol{\tau} = \boldsymbol{\Psi}\Delta\boldsymbol{\tau} \tag{4.15}$$

If $\Delta\boldsymbol{\kappa} \geqslant \epsilon$, where ϵ is some tolerance, the thrust guess is insufficient and needs to be corrected. This can be done by rearranging Equation 4.15 to

$$\Delta\boldsymbol{\tau} = \boldsymbol{\Psi}^{-1}\Delta\boldsymbol{\kappa}_k$$

However, $\boldsymbol{\Psi}$ is not a square matrix, representing an over-determined system, and the inverse cannot be taken directly. One approximation can be found using the least-squares fit shown by rearranging Equation 4.15 to[7]

$$\boldsymbol{\Psi}\Delta\boldsymbol{\tau} = \Delta\boldsymbol{\kappa}_k$$
$$\boldsymbol{\Psi}^T\boldsymbol{\Psi}\Delta\boldsymbol{\tau} = \boldsymbol{\Psi}^T\Delta\boldsymbol{\kappa}_k$$
$$\Rightarrow \quad \Delta\boldsymbol{\tau} = \left[\boldsymbol{\Psi}^T\boldsymbol{\Psi}\right]^{-1}\boldsymbol{\Psi}^T\Delta\boldsymbol{\kappa}_k \tag{4.16}$$

Now, it just needs to be shown that $\boldsymbol{\Psi}^T\boldsymbol{\Psi}$ is invertible. For any matrix $A \in \mathbb{R}^{p\times q}$ that is rank q where $q < p$, $A^T A$ is rank q (full rank) and therefore invertible.[9] Because $\boldsymbol{\Psi}$ is a $p \times q$ matrix where $q < p$, $\boldsymbol{\Psi}^T\boldsymbol{\Psi}$ is invertible if $\boldsymbol{\Psi}$ is rank q (full column rank). This occurs when there are q linearly independent states (dimension of $\boldsymbol{\tau}$) being estimated or, in this specific case, when τ_r, τ_θ, and τ_h are linearly independent. Because the thrust components lie entirely along their respective bases (τ_i acts in the $\hat{i}$ direction) and $\left\{\hat{r},\ \hat{\theta},\ \hat{h}\right\}$ is an orthogonal basis for $\mathbb{R}^3$ describing the LVLH frame, $\hat{r}$, $\hat{\theta}$, and $\hat{h}$ are linearly independent,

therefore τ_r, τ_θ, and τ_h are linearly independent. So $\boldsymbol{\Psi}$ is rank q (full column rank), and therefore $\boldsymbol{\Psi}^T\boldsymbol{\Psi}$ is invertible. Now, the thrust correction can be defined as a function of the change in the orbital elements $\Delta\boldsymbol{\kappa}_k$.

Applying the least-squares approximation (Equation 4.16)

$$\Delta\boldsymbol{\tau} = \boldsymbol{\tau} - \tilde{\boldsymbol{\tau}} = \left[\boldsymbol{\Psi}^T\boldsymbol{\Psi}\right]^{-1}\boldsymbol{\Psi}^T\Delta\boldsymbol{\kappa}_k$$
$$\Rightarrow \quad \boldsymbol{\tau} = \tilde{\boldsymbol{\tau}}^- + \left[\boldsymbol{\Psi}^T\boldsymbol{\Psi}\right]^{-1}\boldsymbol{\Psi}^T\Delta\boldsymbol{\kappa}_k$$

where $\boldsymbol{\tau}^-$ is the thrust estimate before updating. The updated estimate $(\boldsymbol{\tau}^+)$ is then

$$\tilde{\boldsymbol{\tau}}^+ = \boldsymbol{\tau} = \tilde{\boldsymbol{\tau}}^- + \left[\boldsymbol{\Psi}^T\boldsymbol{\Psi}\right]^{-1}\boldsymbol{\Psi}^T\Delta\boldsymbol{\kappa}_k$$

and the process is repeated until $\Delta\boldsymbol{\kappa}_k \approx 0$ or equivalently $\Delta\boldsymbol{\tau} \approx 0$ (to some tolerance) implying

$$\Delta\boldsymbol{\tau} = \boldsymbol{\tau} - \tilde{\boldsymbol{\tau}} \approx 0 \quad \Rightarrow \quad \tilde{\boldsymbol{\tau}} \approx \boldsymbol{\tau}$$

determining the constant thrust vector used for the maneuver. The numerical calculation of $\boldsymbol{\Psi}$ is detailed in Section 7.

4.3. TIME-VARYING THRUST VECTOR

For time-varying thrust vectors, attitude knowledge would be required to accurately estimate the applied thrust. This means that the thrust vector direction is no longer uncertain but instead a known vector, therefore, the only unknown is the magnitude of the applied thrust force, $||\boldsymbol{\tau}||$ (which is assumed constant from $t_0 \rightarrow t_k$). Because the thrust magnitude is scalar, it can be removed from the integral similarly to the constant thrust vector as

$$\Delta \boldsymbol{\kappa}_k = \int_{t_0}^{t_k} \boldsymbol{\Phi}'(t) \Delta \boldsymbol{\tau}(t) \, dt$$

$$= ||\Delta \boldsymbol{\tau}|| \int_{t_0}^{t_k} \boldsymbol{\Phi}'(t) \frac{\Delta \boldsymbol{\tau}(t)}{||\Delta \boldsymbol{\tau}||} \, dt$$

$$= ||\Delta \boldsymbol{\tau}|| \boldsymbol{\Psi} \tag{4.17}$$

where $\boldsymbol{\tau}/||\boldsymbol{\tau}||$ is the unit vector of the thrust vector with respect to the LVLH reference frame (which is required to be known/estimated with attitude data collected throughout the maneuver). Equation 4.17 can be rearranged using the least-squares method resulting in

$$||\Delta \boldsymbol{\tau}|| = ||\boldsymbol{\tau}|| - ||\tilde{\boldsymbol{\tau}}|| = \left[\boldsymbol{\Psi}^T \boldsymbol{\Psi} \right]^{-1} \boldsymbol{\Psi}^T \Delta \boldsymbol{\kappa}_k$$

the corrected thrust magnitude estimated is then

$$||\tilde{\boldsymbol{\tau}}||^+ = ||\tilde{\boldsymbol{\tau}}||^- + \left[\boldsymbol{\Psi}^T \boldsymbol{\Psi} \right]^{-1} \boldsymbol{\Psi}^T \Delta \boldsymbol{\kappa}_k$$

and again, the process is repeated until $\Delta \boldsymbol{\kappa}_k \approx 0$ or equivalently $||\Delta \boldsymbol{\tau}|| \approx 0$ (to some tolerance) meaning

$$||\Delta \boldsymbol{\tau}|| = ||\boldsymbol{\tau}|| - ||\tilde{\boldsymbol{\tau}}|| = 0 \qquad \Rightarrow \qquad ||\tilde{\boldsymbol{\tau}}|| = ||\boldsymbol{\tau}||$$

determining the magnitude of the thrust vector used for the maneuver.

4.4. ALGORITHM FLOW CHART

The corrector requires an initial thrust guess ($\tilde{\boldsymbol{\tau}}$), the initial and final state measurements ($\boldsymbol{\kappa}_0$ and $\boldsymbol{\kappa}_f$), and the maneuver burn length (t_f). The iterative processes for the thrust determination process is shown in Figure 4.2.
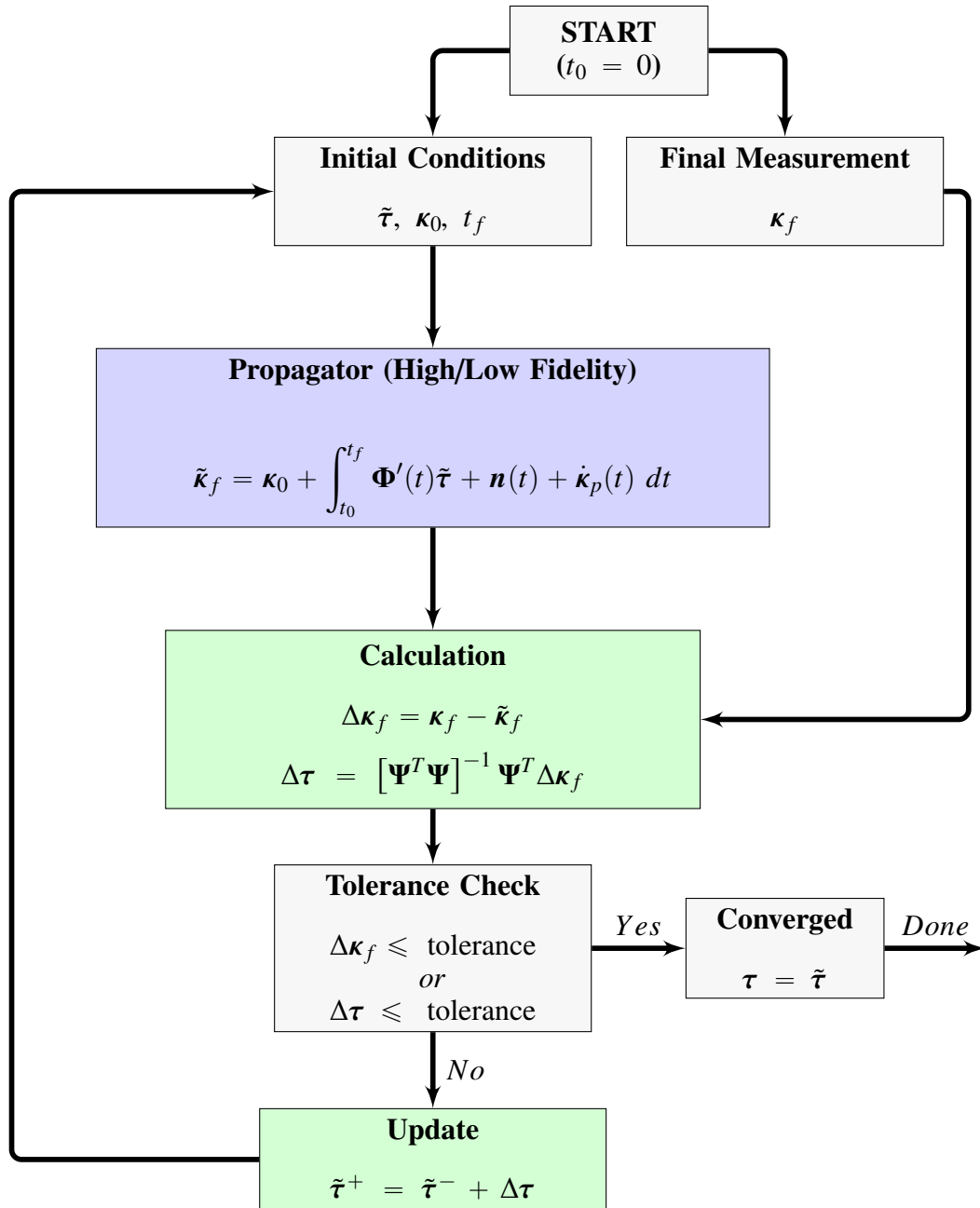
Figure 4.2. Thrust Determination Iteration Loop (Constant Thrust Vector)

5. MANEUVER OPTIONS (OBJECTIVE #2)

5.1. DIRECT MEASUREMENT WITH ACCELEROMETER

The acceleration due to the thrust applied to the satellite can be measured using an accelerometer. If both the acceleration due to the thrust and the mass of the satellite are known, Newton's second law

$$F = mA$$

can be used to directly determine thrust. In the case of the APEX mission, the mass of the satellite can be directly measured. On Earth's surface, a stationary accelerometer is supported by a force equal to the gravitational force. This means the measurements will reflect the accelerometer bias and the acceleration to due the force of gravity. This won't occur in space, therefore the accelerometer will only indicate the accelerometer bias unless an external force (i.e. a propulsive maneuver and other perturbations) is applied.[10]

The main issue with using accelerometers is the bias. When using electric, low-thrust, propulsion systems, the bias is generally larger than the acceleration due to thrust and therefore cannot accurately quantify thrust. The accelerometers that have the required accuracy are expensive and often excessive for university satellites like the APEX mission. The APEX mission uses the ADXL355 3-axis accelerometer by Analog Devices Inc. The specifications of this accelerometer are shown in Table 5.1.

The typical sensitivity of this accelerometer for the ± 2 option is 256,000 LSB/g where LSB refers to least significant bit and g is gravity or 9.81 m/s^2. In order to determine the applied thrust within $\pm 10\%$, an accelerometer should be able to detect at a minimum 10% of the acceleration due to the thrust applied to the satellite. This accelerometer is

Table 5.1. ADXL355 Digital Output Specifications

$T_A = 25°C$, $V_{SUPPLY} = 3.3$ V, x-axis acceleration and y-axis acceleration = 0 g, and z-axis acceleration = 1 g, and output data rate (ODR) = 500 Hz, unless otherwise noted. Note that multifunction pin names may be referenced by their relevant function only.

Parameter	Test Conditions/Comments	Min	Typ	Max	Unit
SENSOR INPUT	Each axis				
Output Full Scale Range (FSR)	User selectable		±2.048		g
			±4.096		g
			±8.192		g
Nonlinearity	±2 g		0.1		% FS
Cross Axis Sensitivity			1		%
SENSITIVITY	Each axis				
X-Axis, Y-Axis, and Z-Axis Sensitivity	±2 g	235,520	256,000	276,480	LSB/g
	±4 g	117,760	128,000	138,240	LSB/g
	±8 g	58,880	64,000	69,120	LSB/g
X-Axis, Y-Axis, and Z-Axis Scale Factor	±2 g		3.9		µg/LSB
	±4 g		7.8		µg/LSB
	±8 g		15.6		µg/LSB
Sensitivity Change due to Temperature	−40°C to +125°C		±0.01		%/°C
0 g OFFSET	Each axis, ±2 g				
X-Axis, Y-Axis, and Z-Axis 0 g Output		−75	±25	+75	mg
0 g Offset vs. Temperature (X-Axis, Y-Axis, and Z-Axis)[1]	−40°C to +125°C	−0.15	±0.02	+0.15	mg/°C
Repeatability[2]	X-axis and y-axis		±3.5		mg
	Z-axis		±9		mg
Vibration Rectification[3]	±2 g range, in a 1 g orientation, offset due to 2.5 g rms vibration		<0.4		g
NOISE DENSITY	±2 g				
X-Axis, Y-Axis, and Z-Axis			25		µg/√Hz
Velocity Random Walk	X-axis and y-axis		9		µm/sec/√Hr
	Z-axis		13		µm/sec/√Hr
OUTPUT DATA RATE AND BANDWIDTH					
Low-Pass Filter Passband Frequency	User programmable, Register 0x28	1		1000	Hz
High-Pass Filter Passband Frequency When Enabled (Disabled by Default)	User programmable, Register 0x28 for 4 kHz ODR	0.0095		10	Hz

capable of determining an acceleration of

$$\text{Sensitivity} = 256000 \text{ LSB/g} \Rightarrow 3.90625 \times 10^{-6} \text{ g/LSB}$$

The minimum detectable acceleration (A_{min}) is the acceleration valued at one least significant bit or

$$A_{min} = 3.90625 \times 10^{-6} \text{ g} = 3.83203 \times 10^{-5} \text{ m/s}^2$$

Because it is required to determine the thrust within $\pm10\%$, the minimum detectable acceleration must be capable of measuring 10% of the expected applied thrust, therefore the minimum detectable force is

$$F_{min} = mA_{min} = 8.306 \times 3.83203 \times 10^{-5} = 3.18288 \times 10^{-4} \text{ N}$$

where m is the wet mass of the APEX satellite. The measured thrust is then defined as

$$\tau = F \pm F_{error} \quad \text{where} \quad F_{error} < F_{min}$$

and F_{error} is less than 10% of the expected thrust (τ), therefore

$$F_{min} \geqslant 10\%\tau$$

and rearranging, the minimum measurable thrust is

$$\tau = \frac{F_{min}}{10\%} = 3.18288 \text{ mN}$$

Unfortunately, this force is not small enough to directly measure the APEX electric propulsion system, which only produces 0.25 mN of thrust. These calculations don't include startup bias and nonlinearity errors, therefore another method must be used to quantify the thrust of electric propulsion systems.

5.2. MANEUVER SELECTION

One of the challenges for small satellite design is the limited space available for propulsion systems. The example analyzed in this study is the Missouri University of Science and Technology Satellite Research Team's (M-SAT) APEX mission. The limited propellant on-board (75 cm^3) requires that the on-orbit thrust quantification be determined with relatively short burn times. It is therefore critically important to formulate a mission

design that implements maneuvers that result in orbit changes of sufficiently large magnitudes for accurately determining the thrust performance. Two types of maneuvers were considered: an attitude changing maneuver and an orbit changing maneuver (in addition to measuring thrust directly with an accelerometer). The mission design was driven by the desire to maximize orbit/attitude changes resulting from each maneuver to accurately determine the thruster performance.

5.2.1. Attitude. Using attitude determination as the primary means by which to quantify thruster performance would require that the thruster be placed in a location with a significant offset from its center of mass; thrusting would then change the attitude and angular rate rather than translating the satellite. A minimum angular rate and/or attitude slew is required, if changes in the attitude/angular rate are to be accurately determined with respect to the noise present in the attitude sensors.

5.2.1.1. Attitude changing maneuver options. An inertial measurement unit (IMU) generally contains a gyroscope and three accelerometers and is typically a leading candidate on smallsats for measuring attitude rates. Ideally the thruster is located to impart the maximum possible torque on the satellite. The limited power on-board requires some satellites (such as APEX) to be Sun pointing, so the thruster orientation was chosen to only produce a moment along the APEX z-axis (shown in Figure 5.1) to rotate the satellite in a manner that keeps the solar panels pointing away from Earth at all times. Figure 5.1 shows the general layout of the 6U APEX satellite with a thruster located such that the maximum amount of torque is generated. The red frame shows the body-fixed axes, the blue line represents the thrust direction, and the orange circle indicates the direction of the moment produced.

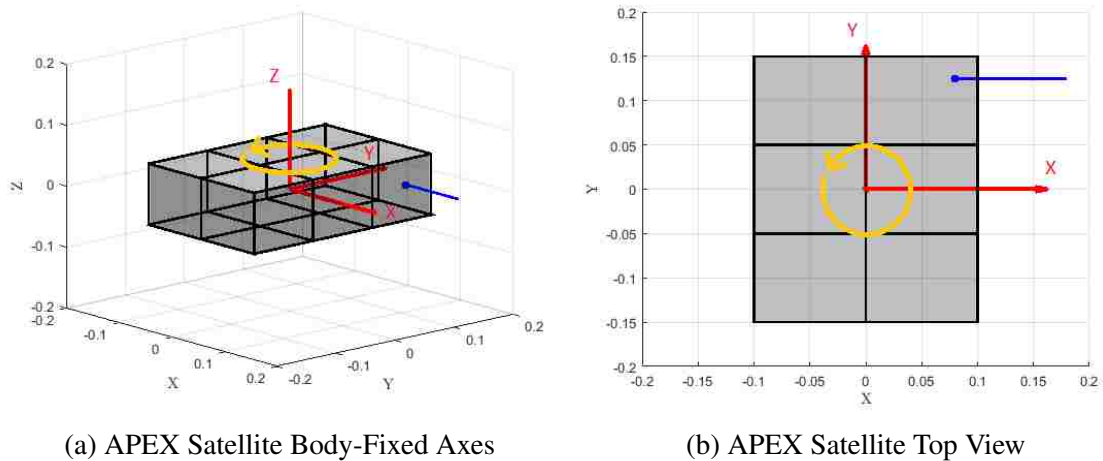| (a) APEX Satellite Body-Fixed Axes | (b) APEX Satellite Top View |

Figure 5.1. Attitude Changing Maneuver Thruster Location

Small satellites, particularly those without deployable solar panels, commonly have power constraints limiting the duration of maneuvers. This would require any maneuvers longer than the maximum duration allowed by the power restrictions to be split into two or more separate maneuvers resulting in a more complex maneuver and allowing for other perturbations to affect the angular rate.

5.2.1.2. Attitude maneuver sensitivity. The IMU gyroscopic sensor chosen for this analysis is the EPSON M-G364 IMU[11], it has an initial error of 0.1 deg/s and an angular random walk of 0.09 deg/$\sqrt{\text{hr}}$, or 0.0015 deg/$\sqrt{\text{sec}}$; with this in mind a satellite would need to be spun to an angular rate of at least 0.21 deg/s, chosen to exceed the gyroscope bias by a factor of two (assuming the attitude rates of the satellite are recorded every ten seconds) to dominate the noise from the sensors. Using the APEX mission as an example, the total burn time required for the satellite to spin up to 0.21 deg/sec would then be approximately 1.06 hours in electric mode and 1.14 seconds in chemical mode. Because of the required length for the electric mode burn and the limited amount of propellant to perform multiple maneuvers, an attitude rate changing maneuver was not considered a desirable option.

5.2.2. Orbit. The orbit changing maneuver option was expanded to three options, an altitude changing maneuver and two orbit plane changes: right ascension of the ascending node (Ω) and inclination (i). These orbital elements are shown in Figure 5.2. In
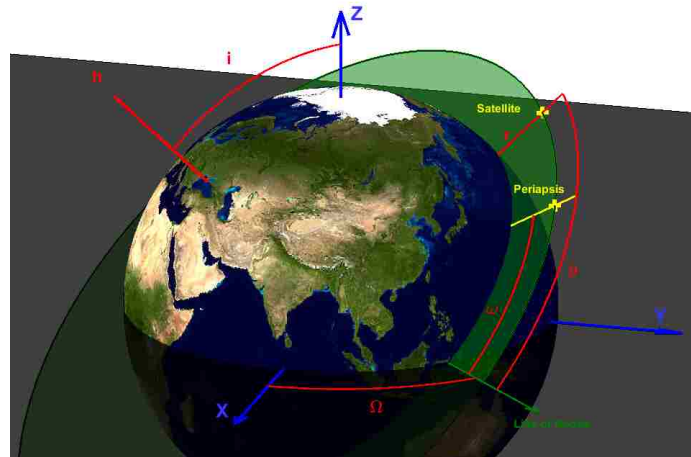
Figure 5.2. Orbital Elements of Interest

assessing each option, it was assumed that APEX will be placed in a low Earth orbit that experiences some significant amount of aerodynamic drag. The orbit changing option logically places the thruster along a body-fixed axis with the origin aligned with the center of mass of APEX. This location/orientation ensures that the thruster, when activated, will not induce a significant torque on the satellite. This layout is shown in Figure 5.3. The red frame shows the body-fixed axes and the blue line represents the thrust direction.
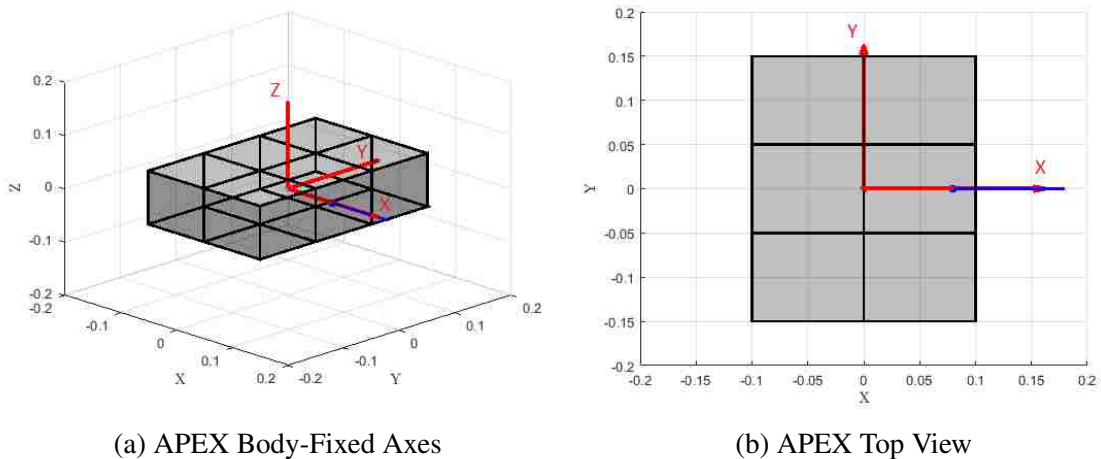
(a) APEX Body-Fixed Axes

(b) APEX Top View

Figure 5.3. Orbit Maneuver Thruster Location

5.2.2.1. Orbital element change maneuver locations. The optimal location to perform each maneuver on orbit must be determined. This is done by examining the Gauss VOP equations and ascertain the on-orbit location that results in the largest orbital element change. The finite maneuvers are then centered about the resulting location to impact the greatest change for a given amount of propellant.

Periapsis Altitude Change. To determine the optimal location to perform a periapsis altitude changing maneuver the equations for perigee and apogee are examined using the Gaussian VOP equations, with perigee and apogee defined as

$$r_p = a(1 - e) \qquad\qquad r_a = a(1 + e)$$

where r_p is the orbit perigee, r_a is the orbit apogee and a and e are the semimajor axis and eccentricity respectively. To increase perigee the semimajor axis needs to increase, but if eccentricity increases the perigee will decrease, so it was decided to perform a maneuver that raises the semimajor axis and decreases eccentricity. Equations 2.1-2.7 show that only the $\hat{r}$ and $\hat{\theta}$ components of thrust affect semimajor axis and eccentricity.

For circular/near circular orbits (eccentricity ≈ 0), it is more beneficial to thrust along the positive $\hat{\theta}$ direction to increase semimajor axis. In order to force the eccentricity to decrease, the following equation must be negative

$$(p + r) \cos{(v)} + re \approx (p + r) \cos{(v)} < 0$$

where v is the true anomaly and r is the radius from Earth's center. This equation is the most negative when $v = 180°$, at least for circular/near circular orbits, therefore, to raise perigee, a finite maneuver should be centered about apogee and performed in the $\hat{\theta}$ direction to optimize fuel consumption.

RAAN/Inclination Change. Considering next orbit plane change maneuvers, in order to demonstrate thruster performance from a RAAN/inclination change, the Two-Body Gaussian VOP Equations were used to determine the optimal location to perform the maneuvers, where optimal is define as maximizing the orbit plane rotation, maximizing change in RAAN and inclination require the Gauss VOP equations to be maximized, specifically

$$\frac{d\Omega}{dt} = \frac{r\sin(\theta)}{h\sin(i)} \qquad\qquad \frac{di}{dt} = \frac{r\cos(\theta)}{h}$$

By inspection it is clear that the optimal location for inclination is at an argument of latitude (θ) of $0°$ or $180°$, especially when considering circular/near circular orbits ($r = $ constant). Using Equation 2.4, it can be shown that there is a larger RAAN rate when the orbit plane is closer to the equatorial plane and when the argument of latitude is $\pm 90°$. The locations for finite maneuvers to be centered about, for maximum orbital element change, can be seen in Table 5.2.

Table 5.2. Maneuver Locations

	Maneuver Center Location
Δr_p	$\nu = 180°$
$\Delta\Omega$	$\theta = \pm 90°$
Δi	$\theta = 0°$ or $180°$

5.2.2.2. Maneuver sensitivity to state error. In Section 4 the thrust determination algorithms rely upon measuring the change in orbital elements resulting from a maneuver, therefore the accuracy of the thrust determination relies on the accuracy of the measured orbital element change. The preferred orbital maneuver would be the one that minimizes the difference between the true and estimated orbital element change in the presence of position and velocity measurement uncertainty. This ensures that poor state estimation will have a minimal effect on thrust estimation.

To determine the maneuver that minimizes the effect of state estimation uncertainty the three maneuvers are compared using a probability of success calculation. Initially, a nominal maneuver is simulated and used as the truth. From this, the initial and final Cartesian states are obtained as well as the initial (κ_0) and final (κ_f) Keplerian states. Then, N pairs of random samples of the satellite's position and velocity components are generated at the beginning and end of the maneuver, according to the noise from the GPS receiver (assuming the error is normally distributed). These random samples are transformed into N initial ($\tilde{\kappa}_0$) and final ($\tilde{\kappa}_f$) Keplerian states. The difference between the true orbital element change ($\Delta\kappa$) and noisy orbital element change ($\Delta\tilde{\kappa}$) is calculated, if the absolute value of the difference, $|\Delta\kappa - \Delta\tilde{\kappa}|$, is less than or equal to 10% of the truth, the estimate is deemed valid, and the run is a success, or

$$ S = P_R\left(|\Delta\kappa - \Delta\tilde{\kappa}| \leqslant 0.1\Delta\kappa\right) \qquad \text{where} \quad \begin{aligned} \Delta\kappa &= \kappa_f - \kappa_0 \\ \Delta\tilde{\kappa} &= \tilde{\kappa}_f - \tilde{\kappa}_0 \end{aligned} $$

The sensitivity analysis was performed by numerically integrating the Two-Body VOP equations using the same thrust magnitude and maneuver burn time with the maneuvers centered about the locations specified in Table 5.2 to obtain a true state change. A Monte Carlo analysis was then run with one million random position and velocity samples using a small position and velocity uncertainty.

As the specific mission orbit is not yet known, a generic set of low Earth orbit (LEO) initial conditions were arbitrarily selected and are shown in Table 5.3. The true anomaly for the start of the maneuver is different for each maneuver and dependent upon the maneuver center locations defined in Table 5.2. Two-body dynamics are used for the entirety of this section to obtain a close approximation without the computational burden of using a higher fidelity dynamical model. This also has the convenient result of semimajor axis, eccentricity, and true anomaly remaining constant when performing RAAN or inclination changing maneuvers, while inclination and RAAN remain constant when performing perigee altitude

changing maneuvers. Arbitrarily selecting a small root mean square (RMS) position and

Table 5.3. Initial Conditions

a (km)	e	i (deg)	Ω (deg)	ω (deg)
6779.899	0.005	45	45	90

velocity uncertainty with standard deviations of

$$\sigma_{x,rms} = 1.5 \text{ m} \qquad\qquad \sigma_{v,rms} = 10 \text{ mm/s}$$

where x and v represent position and velocity respectively. The position and velocity component standard deviations are

$$\sigma_{x,rms} = \sqrt{\sigma_x^2 + \sigma_y^2 + \sigma_z^2}$$

$$\Rightarrow \sigma_x = \sigma_y = \sigma_z = \frac{\sigma_{x,rms}}{\sqrt{3}} = 0.866 \text{ m}$$

$$\sigma_{v,rms} = \sqrt{\sigma_{\dot{x}}^2 + \sigma_{\dot{y}}^2 + \sigma_{\dot{z}}^2}$$

$$\Rightarrow \sigma_{\dot{x}} = \sigma_{\dot{y}} = \sigma_{\dot{z}} = \frac{\sigma_{v,rms}}{\sqrt{3}} = 5.774 \text{ mm/s}$$

assuming each axis exhibits the same standard deviation. The preferred maneuver will be the maneuver with the highest probability of success.

Altitude Change. Recall the perigee raising maneuver is centered about the apogee ($v = 180°$) and is calculated via

$$r_p = a(1 - e)$$

The changing orbital element of interest will be the perigee altitude (not semimajor axis and eccentricity separately) in order to bypass the singularity in the Gaussian VOP equations for small eccentricity. The change in perigee is then

$$\Delta r_p = a_f(1 - e_f) - a_0(1 - e_0)$$

$$= (a_f - a_0) - (a_f e_f - a_0 e_0)$$

where the subscripts 0 and f correspond to the beginning and end of the maneuver respectively.

Because the semimajor axis and eccentricity are not expressed in terms of the Cartesian reference frame, the random variables x, y, z, $\dot{x}$, $\dot{y}$, and $\dot{z}$ must be converted to a and e. This is done by using

$$a = \frac{-\mu}{||\mathbf{v}||^2 - 2\mu||\mathbf{x}||^{-1}}$$

$$e = \left\| \left(\frac{||\mathbf{v}||^2}{\mu} - \frac{1}{||\mathbf{x}||} \right) \mathbf{x} - \left(\mathbf{x} \bullet \mathbf{v} \right) \frac{\mathbf{v}}{\mu} \right\|$$

where
$$\mathbf{x} = \begin{bmatrix} x \\ y \\ z \end{bmatrix} \quad \text{and} \quad \mathbf{v} = \begin{bmatrix} \dot{x} \\ \dot{y} \\ \dot{z} \end{bmatrix}$$

where μ is the gravitational constant.[6] Now Δr_p is a function of random variables x, y, z, $\dot{x}$, $\dot{y}$, and $\dot{z}$. Let (g_{alt}) be the constraint requiring the estimated perigee change be within $\pm 10\%$ of the true perigee change, the system therefore fails if $g_{alt}(\mathbf{x}, \mathbf{v}) \leqslant 0$ which, for a perigee altitude change, is defined as

$$g_{alt}(\mathbf{x}, \mathbf{v}) = 0.1\Delta r_p - \left| \Delta r_p - \Delta \tilde{r}_p \right|$$

$$= 0.1\Delta r_p - \left| \Delta r_p - \left[a_f - a_0 \right] + \left[a_f e_f - a_0 e_0 \right] \right|$$

$$= 0.1\Delta r_p - \left| \Delta r_p - \left[\frac{-\mu}{||\mathbf{v}_f||^2 - 2\mu||\mathbf{x}_f||^{-1}} - \frac{-\mu}{||\mathbf{v}_0||^2 - 2\mu||\mathbf{x}_0||^{-1}} \right] + \ldots \right.$$

$$\ldots + \left[\frac{-\mu}{||\mathbf{v}_f||^2 - 2\mu||\mathbf{x}_f||^{-1}} \left\| \left(\frac{||\mathbf{v}_f||^2}{\mu} - \frac{1}{||\mathbf{x}_f||} \right) \mathbf{x}_f - \left(\mathbf{x}_f \bullet \mathbf{v}_f \right) \frac{\mathbf{v}_f}{\mu} \right\| \right] + \ldots$$

$$\left. \ldots + \frac{\mu}{||\mathbf{v}_0||^2 - 2\mu||\mathbf{x}_0||^{-1}} \left\| \left(\frac{||\mathbf{v}_0||^2}{\mu} - \frac{1}{||\mathbf{x}_0||} \right) \mathbf{x}_0 - \left(\mathbf{x}_0 \bullet \mathbf{v}_0 \right) \frac{\mathbf{v}_0}{\mu} \right\| \right] \right|$$

where Δr_p is the true perigee change and $\Delta \tilde{r}_p$ is the perigee change with position and velocity uncertainty.

RAAN Change. The RAAN change is defined as

$$\Delta\Omega = \Omega_f - \Omega_0 \tag{5.1}$$

Ω can be expressed in terms of Cartesian elements by

$$\Xi = \hat{z} \times \boldsymbol{h} = \hat{z} \times (\boldsymbol{x} \times \boldsymbol{v}) = \begin{bmatrix} \xi_1 & \xi_2 & \xi_3 \end{bmatrix}^T$$

$$\Omega = \cos^{-1}\left(\frac{\xi_1}{||\Xi||}\right)$$

where $\hat{z}$ is the the z-axis of the Earth-centered inertial (ECI) reference frame and $\boldsymbol{h}$ is the orbit angular moment vector. Expanding these results in

$$\Xi = \begin{bmatrix} 0 \\ 0 \\ 1 \end{bmatrix} \times \left(\begin{bmatrix} x \\ y \\ z \end{bmatrix} \times \begin{bmatrix} \dot{x} \\ \dot{y} \\ \dot{z} \end{bmatrix} \right) = \begin{bmatrix} x\dot{z} - z\dot{x} \\ y\dot{z} - z\dot{y} \\ 0 \end{bmatrix}$$

$$\Rightarrow \quad \Omega = \cos^{-1}\left(\frac{x\dot{z} - z\dot{x}}{\sqrt{(x\dot{z} - z\dot{x})^2 + (y\dot{z} - z\dot{y})^2}}\right)$$

Substituting back into Equation 5.1

$$\Delta\Omega = \cos^{-1}\left(\frac{x_f\dot{z}_f - z_f\dot{x}_f}{\sqrt{(x_f\dot{z}_f - z_f\dot{x}_f)^2 + (y_f\dot{z}_f - z_f\dot{y}_f)^2}}\right) - \ldots$$

$$\ldots - \cos^{-1}\left(\frac{x_0\dot{z}_0 - z_0\dot{x}_0}{\sqrt{(x_0\dot{z}_0 - z_0\dot{x}_0)^2 + (y_0\dot{z}_0 - z_0\dot{y}_0)^2}}\right)$$

Including the constraint (g_Ω) that the RAAN change must be within $\pm 10\%$ of the true RAAN change, the system fails if $g_\Omega(\boldsymbol{x}, \boldsymbol{v}) \leqslant 0$ where $g_\Omega(\boldsymbol{x}, \boldsymbol{v})$ is defined as

$$g_\Omega(\boldsymbol{x}, \boldsymbol{v}) = 0.1\Delta\Omega - \left|\Delta\Omega - \Delta\tilde{\Omega}\right|$$

$$= 0.1\Delta\Omega - \left|\Delta\Omega - \cos^{-1}\left(\frac{x_f \dot{z}_f - z_f \dot{x}_f}{\sqrt{\left(x_f \dot{z}_f - z_f \dot{x}_f\right)^2 + \left(y_f \dot{z}_f - z_f \dot{y}_f\right)^2}}\right) + \ldots\right.$$

$$\left. \ldots + \cos^{-1}\left(\frac{x_0 \dot{z}_0 - z_0 \dot{x}_0}{\sqrt{\left(x_0 \dot{z}_0 - z_0 \dot{x}_0\right)^2 + \left(y_0 \dot{z}_0 - z_0 \dot{y}_0\right)^2}}\right)\right.$$

where $\Delta\Omega$ is the true RAAN change and $\Delta\tilde{\Omega}$ is the RAAN change with position and velocity uncertainty.

Inclination Change. The inclination change is defined as

$$\Delta i = i_f - i_0 \tag{5.2}$$

Expressing inclination in terms of the Cartesian elements with respect to the ECI reference frame gives

$$\boldsymbol{h} = \boldsymbol{x} \times \boldsymbol{v} = \begin{bmatrix} h_1 & h_2 & h_3 \end{bmatrix}^T$$

$$i = \cos^{-1}\left(\frac{h_3}{\|\boldsymbol{h}\|}\right)$$

this expands to

$$\boldsymbol{h} = \begin{bmatrix} x \\ y \\ z \end{bmatrix} \times \begin{bmatrix} \dot{x} \\ \dot{y} \\ \dot{z} \end{bmatrix} = \begin{bmatrix} y\dot{z} - z\dot{y} \\ z\dot{x} - x\dot{z} \\ x\dot{y} - y\dot{x} \end{bmatrix}$$

$$\Rightarrow \quad i = \cos^{-1}\left(\frac{x\dot{y} - y\dot{x}}{\sqrt{\left(y\dot{z} - z\dot{y}\right)^2 + \left(z\dot{x} - x\dot{z}\right)^2 + \left(x\dot{y} - y\dot{x}\right)^2}}\right) \tag{5.3}$$

Substituting Equation 5.3 into Equation 5.2 gives

$$\Delta i = \cos^{-1}\left(\frac{x_f \dot{y}_f - y_f \dot{x}_f}{\sqrt{\left(y_f \dot{z}_f - z_f \dot{y}_f\right)^2 + \left(z_f \dot{x}_f - x_f \dot{z}_f\right)^2 + \left(x_f \dot{y}_f - y_f \dot{x}_f\right)^2}}\right) - \ldots$$

$$\ldots - \cos^{-1}\left(\frac{x_0 \dot{y}_0 - y_0 \dot{x}_0}{\sqrt{\left(y_0 \dot{z}_0 - z_0 \dot{y}_0\right)^2 + \left(z_0 \dot{x}_0 - x_0 \dot{z}_0\right)^2 + \left(x_0 \dot{y}_0 - y_0 \dot{x}_0\right)^2}}\right)$$

Including the constraint (g_i) that the inclination change must be within $\pm 10\%$ of the true inclination change, the system fails if $g_i(\boldsymbol{x}, \boldsymbol{v}) \leqslant 0$ where $g_i(\boldsymbol{x}, \boldsymbol{v})$ is defined as

$$g_i(\boldsymbol{x}, \boldsymbol{v}) = 0.1\Delta i - \left|\Delta i - \Delta \tilde{i}\right|$$

$$= 0.1\Delta i - \left| \Delta i - \ldots \right.$$

$$\ldots - \cos^{-1}\left(\frac{x_f \dot{y}_f - y_f \dot{x}_f}{\sqrt{\left(y_f \dot{z}_f - z_f \dot{y}_f\right)^2 + \left(z_f \dot{x}_f - x_f \dot{z}_f\right)^2 + \left(x_f \dot{y}_f - y_f \dot{x}_f\right)^2}}\right) + \ldots$$

$$\left. \ldots + \cos^{-1}\left(\frac{x_0 \dot{y}_0 - y_0 \dot{x}_0}{\sqrt{\left(y_0 \dot{z}_0 - z_0 \dot{y}_0\right)^2 + \left(z_0 \dot{x}_0 - x_0 \dot{z}_0\right)^2 + \left(x_0 \dot{y}_0 - y_0 \dot{x}_0\right)^2}}\right)\right|$$

where Δi is the true inclination change and $\Delta \tilde{i}$ is the inclination change with position and velocity uncertainty.

Results. As a summary, the three maneuvers tested were: a perigee altitude change, a RAAN change, and an inclination change. These maneuvers were performed with a constant thrust vector with respect to the LVLH frame with a burn duration of 2300 seconds centered about the respective locations determined in Section 5.2.2.1. A Monte Carlo simulation was run with a position and velocity RMS uncertainties of

$$\sigma_x = 1.5 \text{ m} \qquad\qquad \sigma_v = 10 \text{ mm/s}$$

for one million runs and the probability of success was defined as

$$S = P_R\left(\left|\Delta\kappa - \Delta\tilde{\kappa}\right| \leqslant 0.1\Delta\kappa\right)$$

Table 5.4 shows the probability of success for each of the three maneuvers as well as the true orbital element changes. For the position and velocity uncertainties given above, the maneuver with the highest probability of success is a RAAN changing maneuver (by a slight margin over an inclination changing maneuver).

Table 5.4. Maneuver Probability of Success

	Orbital Element Change	Probability of Success (%)
Δr_p (m)	211.466	59.621
$\Delta\Omega$ (deg)	5.381×10^{-4}	95.891
Δi (deg)	3.812×10^{-4}	95.564

6. NUMERICAL SIMULATION PROCESS

Systems Tool Kit (STK) is a widely-used program marketed by Analytical Graphics, Inc. that models and simulates orbital dynamics with high fidelity including perturbations such as, drag, solar radiation pressure, gravitational harmonics, and third-body gravitational forces. The orbital position and velocity as determined by the STK simulation were used as the "true" satellite states for every simulation. Because the inclination of the orbit is one of the largest factors in quantifying the effects of gravitational harmonics, the simulations were parametrically varied through a range of inclinations from 0-180 degrees.

Three general categories of simulations were run utilizing unperturbed two-body system dynamics, J_2 perturbation only system dynamics, and STK's high-precision orbit propagator (HPOP) system dynamics (gravitational harmonics of degree 21 and order 21 with solar and lunar third-body gravity forces). The APEX parameters used in the STK simulations are:

$$\text{Dry Mass} = 8.2 \text{ kg}$$

$$\text{Wet Mass} = 8.306425 \text{ kg}$$

$$\text{Tank Pressure} = 1.37895 \text{ MPa}$$

$$\text{Tank Volume} = 75 \text{ cm}^3$$

$$\text{Fuel Density} = 1419 \text{ kg/m}^3$$

The orbital elements used in the STK simulation can be seen in Figure 6.1 where the inclination ranged from 0-90 degrees as stated previously. The "true" orbit propagates for one full orbit, then a RAAN changing maneuver centered about an argument of latitude (θ) of 90° is performed, as shown in Figure 6.2, with burn durations of 5 seconds and 1500 seconds for chemical and electric modes respectively, to match the APEX mission's opera-

(a) Low Eccentricity   (b) High Eccentricity

Figure 6.1. STK Initial Conditions

tional plan. Measurements of the state, (x, y, z, $\dot{x}$, $\dot{y}$, $\dot{z}$) with respect to the Earth-centered Inertial (ECI) frame, are collected every second during the maneuvers. The maneuver maintains a constant thrust vector with respect to the LVLH reference frame for the entire maneuver.
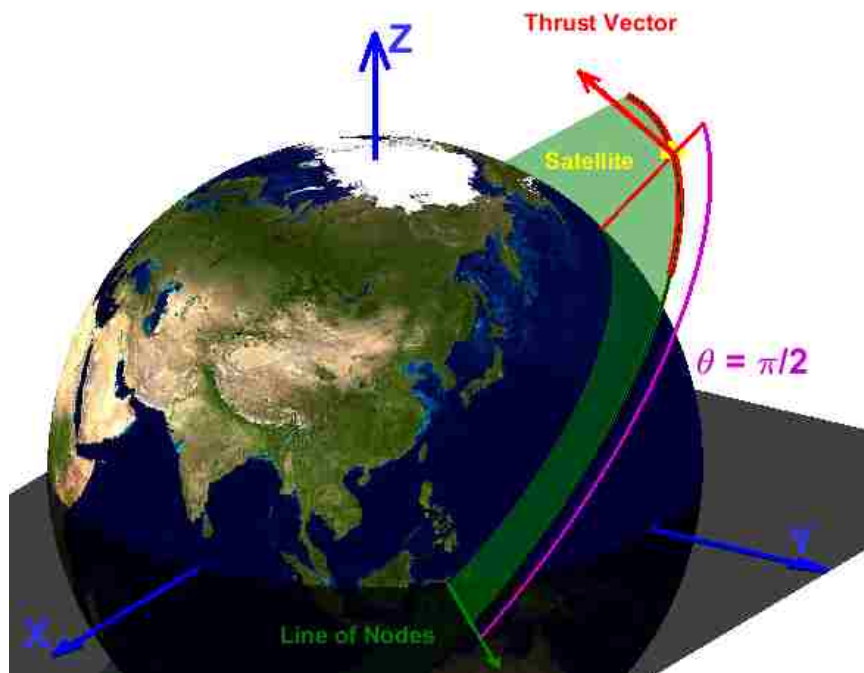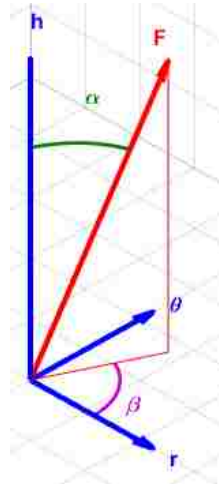

Figure 6.2. Thrust Vector Diagram

Figure 6.3. Thrust Offset Angles

The misalignment of the nozzle and/or attitude error is defined by the offset angles, α and β, as shown in Figure 6.3. The thrust vector used for the simulations, in terms of α, β, and thrust magnitude, is

$$
\tau = \begin{bmatrix} \sin\left(\alpha\right)\cos\left(\beta\right) \\ \sin\left(\alpha\right)\sin\left(\beta\right) \\ \cos\left(\alpha\right) \end{bmatrix} \tau_{mag}
$$

where α and β were arbitrarily selected in order to demonstrate some amount of unknown thrust error. The propulsion system for the APEX mission is capable of both chemical and electric propulsion, and therefore has two engine models in STK; the expected multi-mode propulsion system performance parameters are shown in Table 6.1.[1]

Table 6.1. Engine Model Parameters

	Chemical	Electric
Thrust (N)	1.0	0.00025
I_{sp} (sec)	140.0	412.0

7. RESULTS/COMPARISON

Based on the maneuver sensitivity analyses, the thrust determination methods were tested and compared on RAAN changing maneuvers. Throughout each simulation, all state propagation was performed using STK due to its high-fidelity model. To obtain the uncorrupted true Keplerian states at the beginning and end of each maneuver, the truth model was first propagated with the initial conditions described in Section 6 with a constant thrust vector with respect to the LVLH frame. A (constant) thrust guess ($\tilde{\tau}$), not equal to the true thrust (τ), was applied to the uncorrupted Keplerian states at the beginning of the maneuver (x_0) for 1500 seconds. The thrust estimate and the initial state were used in STK to propagate the state forward in time obtaining estimated Keplerian states at the end of the maneuver ($\tilde{x}_f$). The maneuver length of 1500 seconds was chosen in accordance with the current APEX mission concept of operations. The thrust was then differentially corrected following Section 4.4, where t_0 is the time at the beginning of the maneuver and Ψ was estimated as

$$\Psi = \int_{t_0}^{t_f} \Phi'(t) \, dt \cong \sum_{k=0}^{n-1} \Phi'_k \big(t_{k+1} - t_k \big) = \sum_{k=0}^{n-1} \Phi'_k \Delta t_k \tag{7.1}$$

where n is the number of time steps. For these simulations the time step (Δt) was, after some trial-and-error, selected as one second, therefore

$$\Psi = \sum_{k=0}^{n-1} \Phi'_k \tag{7.2}$$

As a reminder,

$$
\mathbf{\Phi}' =
\begin{bmatrix}
\dfrac{2a^2 e \sin(v)}{hm} & \dfrac{2a^2 p}{hrm} & 0 \\[2ex]
\dfrac{p \sin(v)}{hm} & \dfrac{(p+r)\cos(v)+re}{hm} & 0 \\[2ex]
0 & 0 & \dfrac{r \cos(\theta)}{hm} \\[2ex]
\dfrac{-p \cos(v)}{hem} & \dfrac{(p+r)\sin(v)}{hem} & \dfrac{-r \cos(i) \sin(\theta)}{hm \sin(i)} \\[2ex]
0 & 0 & \dfrac{r \sin(\theta)}{hm \sin(i)} \\[2ex]
\dfrac{p \cos(v)}{hem} & \dfrac{-(p+r)\sin(v)}{hem} & 0
\end{bmatrix}
$$

where $\mathbf{\Phi}'_k$ is $\mathbf{\Phi}'$ evaluated with the Keplerian elements at the kth time step.

Because inclination has a significant effect on the force applied to the satellite due to the gravitational harmonic perturbations the thrust percent error for each of the methods is plotted with respect to the inclination. The thrust percent error is defined as

$$
\%\ ERROR = \frac{\tilde{\tau} - \tau}{\tau} \times 100\%
$$

where a negative percent error represents the estimated thrust converging on a value less than the true thrust. Orbits with two different eccentricities were also considered (0.005 and 0.5) in order to demonstrate the accuracy of the thrust determination for near circular and non-circular orbits.

The chemical mode (high thrust) of the APEX mission is expected to produce a thrust of one newton and a specific impulse of 140 seconds. APEX's electric propulsion mode (low thrust) has a thrust of 0.25 mN and a specific impulse of 412 seconds. The orbital element difference between the truth (κ) and estimated ($\tilde{\kappa}$) final measurement tolerance that define convergence is shown in Table 7.1.

Table 7.1. Thrust Convergence Tolerances

Δa (m)	Δe	Δi (arcsec)	$\Delta \omega$ (arcsec)	$\Delta \Omega$ (arcsec)	Δv (arcsec)
1×10^{-6}	1×10^{-5}	0.1	0.1	0.1	0.1

## 7.1. RESULTS USING TRUE MEASUREMENTS

First, the thrust determination simulations were completed using measurements at the beginning and end of the maneuver without noise to test the accuracy of the methods. A RAAN changing maneuver was performed in STK, as discussed in Section 6, and the uncorrupted initial and final measurements were then fed to the thrust determination algorithm. In order to demonstrate the robustness of the numeric algorithm, a thrust guess ($\tilde{\tau}$) was used with α and β offset angles of $150°$ and $40°$ respectively, and a thrust magnitude guess of 140% of the applied (true) thrust magnitude. The analytic thrust determination method follows the example in Section 3 and assumes the thrust is performed solely in the $\hat{h}$-direction with respect to the LVLH frame; this is a reasonable assumption considering an optimal RAAN changing maneuver would thrust solely in the $\hat{h}$-direction.

7.1.1. High Thrust (1 N). Due to the short timespan of the chemical maneuver, most perturbations have little effect on the orbit; therefore the thigh thrust analytic and numeric thrust determination methods were run using unperturbed Two-Body dynamics and STK's high-precision orbit propagator (HPOP) with gravitational harmonics of degree 21 and order 21 with solar and lunar third body gravitation forces applied. The satellite's true initial states are propagated for a burn duration of five seconds using an estimated thrust ($\tilde{\tau}$) with the STK propagator used to establish the true final Keplerian state to determine the estimated final state. The thrust determination results are very similar for each of the propagation schemes for both low and high eccentric orbits. This can be seen in Figures 7.1 and 7.2 where the difference between the Two-Body and HPOP dynamics is negligible.

The results for the analytic method are all overlapping, therefore it can be concluded that the argument of perigee has little effect for relatively larger thrust with short burns. As expected there are singularities at an inclination of $0°$ and $180°$ where, in the Gauss VOP equations, the RAAN rate is divided by the sine of inclination. This doesn't occur in the
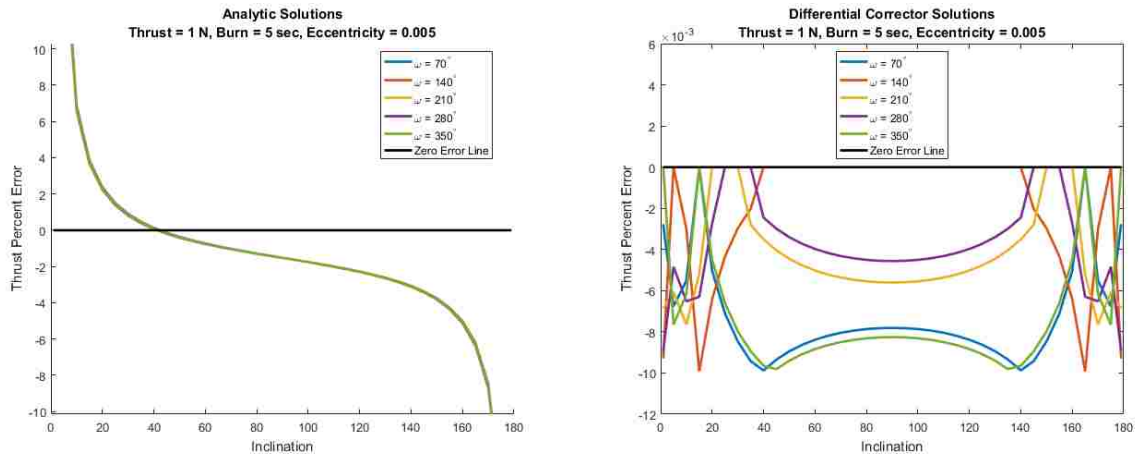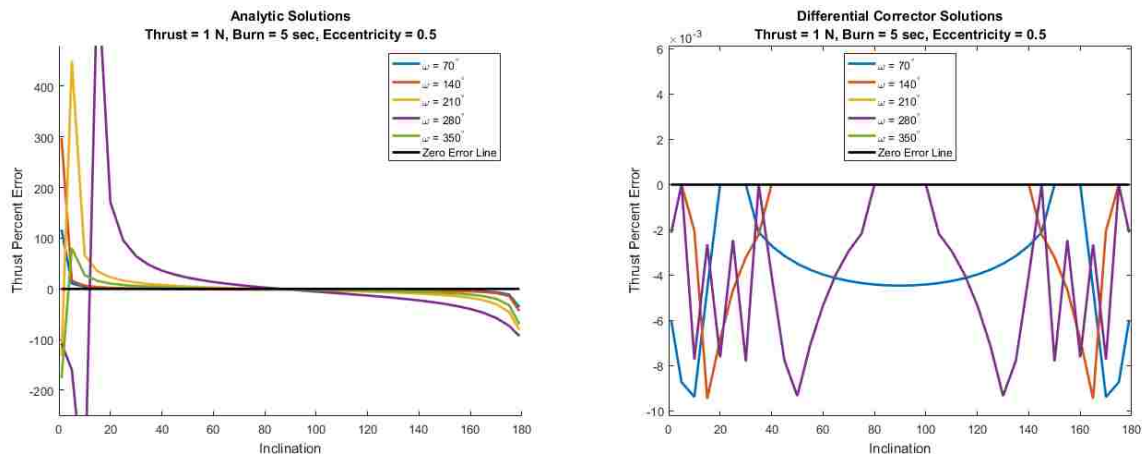
(a) Two-Body Dynamics
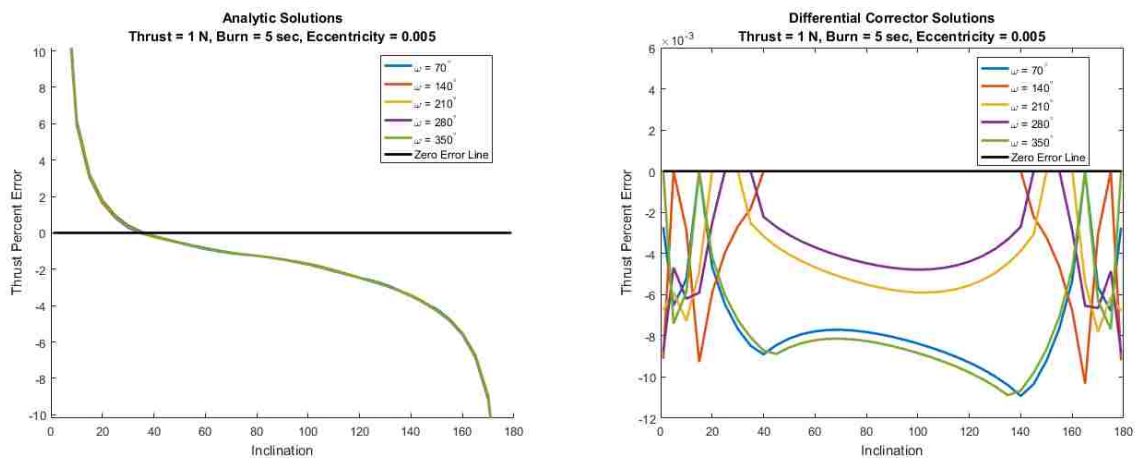
(b) HPOP Dynamics

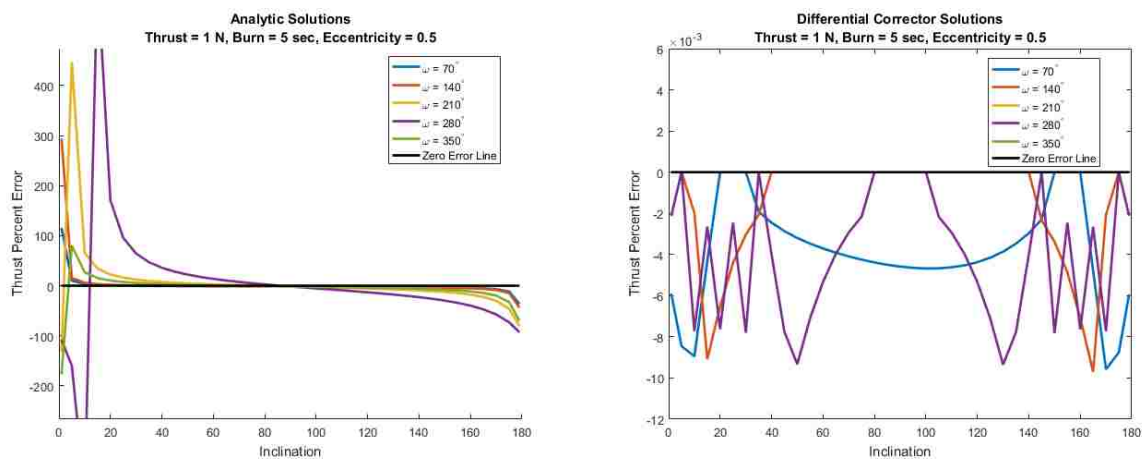Figure 7.1. Chemical Mode Argument of Perigee vs Inclination (Low Eccentricity)

numeric method because inclination is constantly changing throughout the maneuver and is rarely zero. The numeric method converges within 0.0012% of the true thrust for both Two-Body and HPOP dynamics with very similar solutions.

The high eccentricity results follow the same trend as the low eccentricity but the analytic method's thrust determination error is significantly larger for the inclination ranges of $0°$ to $40°$ and $140°$ to $180°$. This could be due to some perturbing forces having a greater effect for the higher eccentric orbit. The numeric method maintained relatively the same

(a) Two-Body Dynamics

(b) HPOP Dynamics

Figure 7.2. Chemical Mode Argument of Perigee vs Inclination (High Eccentricity)

scale accuracy, but argument of perigee had a greater influence with the higher eccentricity orbit and did not always converge on an accurate thrust, and instead diverged. This is shown in Figure 7.2, where $\omega = 210°$ and $\omega = 350°$ lines aren't shown because they did not converge.

7.1.2. Low Thrust (0.25 mN). The electric low-thrust maneuver is long enough for perturbations to have considerable effect, so the thrust determination methods were run with multiple dynamic fidelities to observe the difference perturbations have on the

accuracy of the algorithms. The dynamics used are: unperturbed Two-Body dynamics, J_2 perturbation, and STK's high-precision orbit propagator (HPOP). The satellite's true initial states are propagated for a burn duration of 1500 seconds using an estimated thrust ($\tilde{\tau}$) with the STK propagator used to establish the true final Keplerian state to determine the estimated final state.

7.1.2.1. Two-Body dynamics. Figure 7.3 displays the percent error of the analytic and numeric thrust determination methods for a range of inclinations and arguments of periapsis at both low and high eccentricities for the APEX mission's low (electric) propulsion using Two-Body dynamics.

It is important to note the axis scaling difference between the analytic and numeric methods, the differential corrector solution stays within $\pm 5 \times 10^{-5}\%$ for both the high and low eccentricities. The Two-Body analytic solution remains mostly constant throughout the range of inclinations and incurs more error than the differential corrector. One of the main factors of this is the assumptions made when de-coupling the Gaussian Two-Body VOP equations (circular orbit and constant inclination). The higher eccentricity orbit failed to converge similarly to the chemical mode.
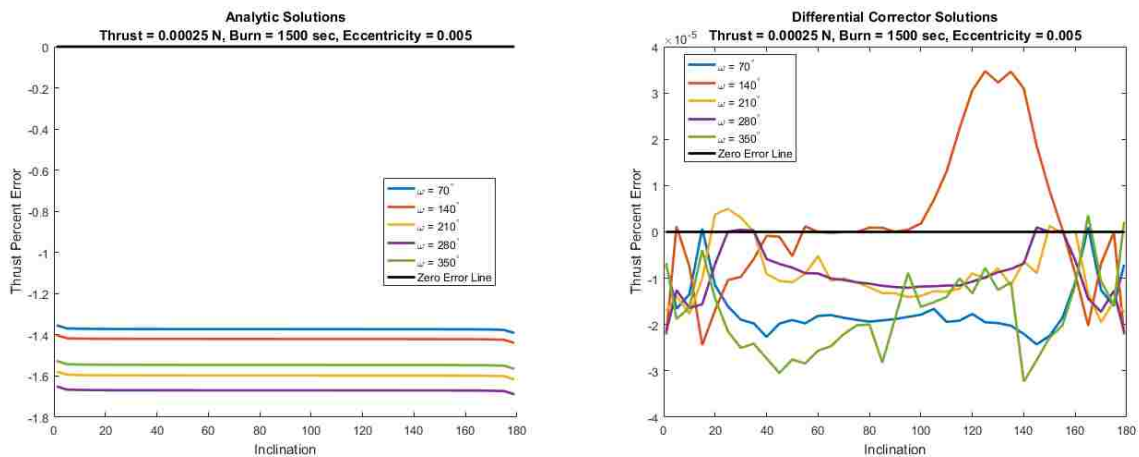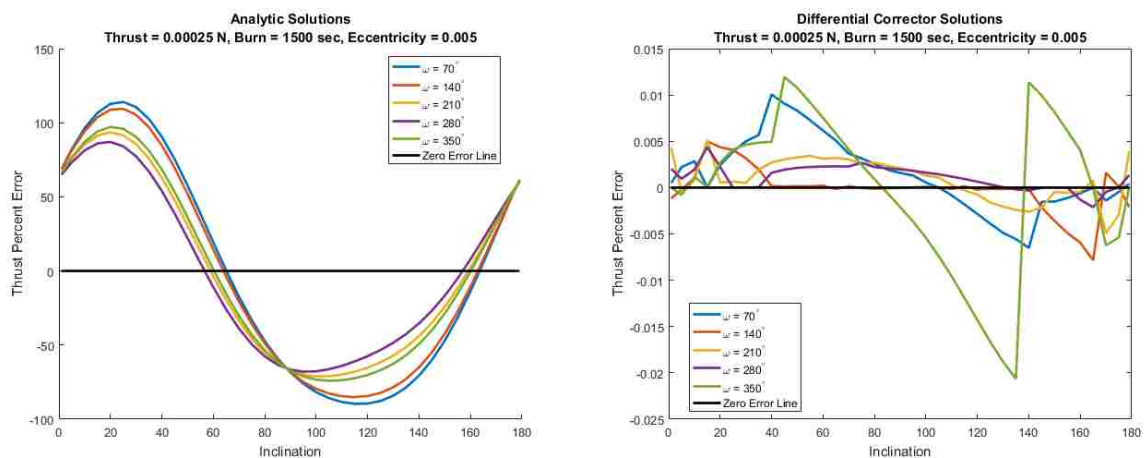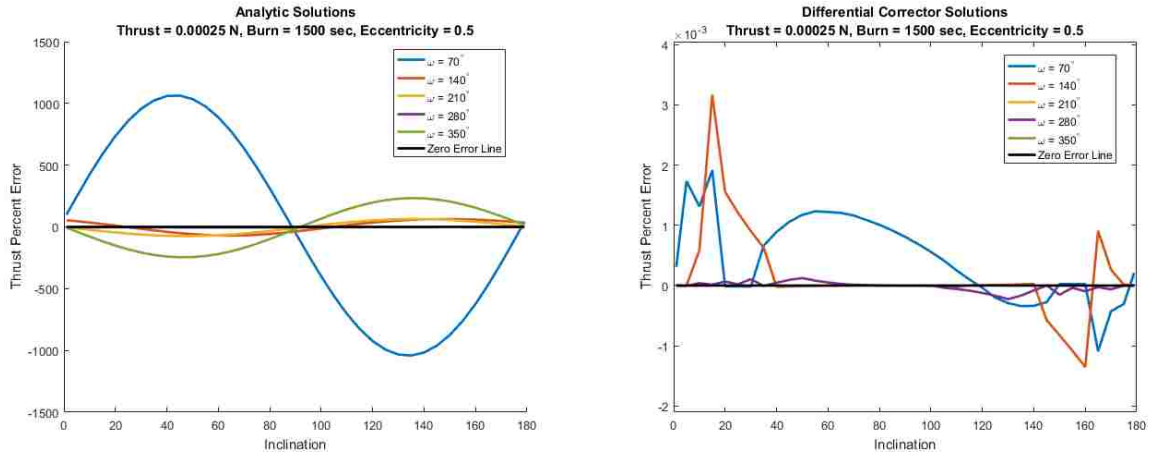

(a) Low Eccentric Orbit
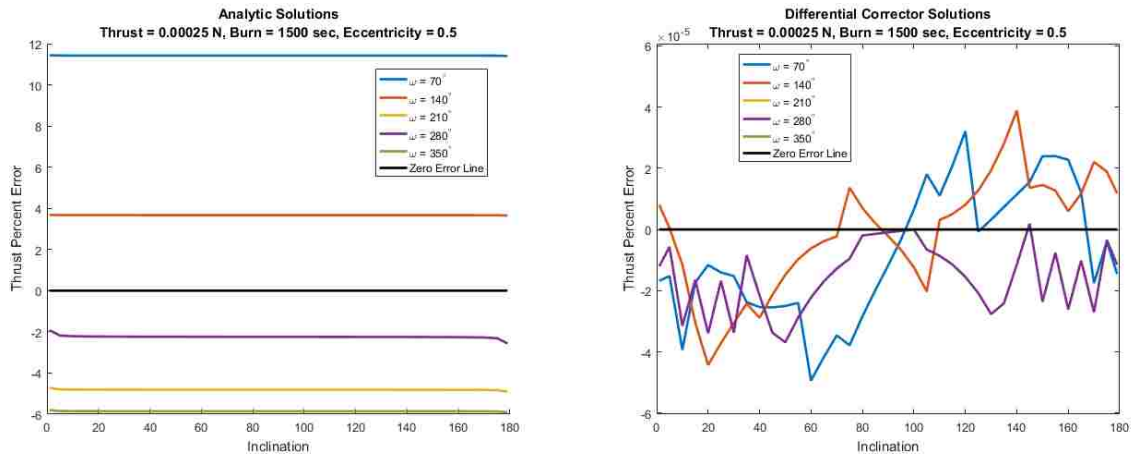
(b) High Eccentric Orbit

Figure 7.3. Two-Body Dynamics: Argument of Perigee vs Inclination

7.1.2.2. J_2 perturbation. Using J_2 dynamics, the analytic method has large errors; this is mostly due to the assumptions made when deriving the analytic equations (constant inclination and circular orbit). Once perturbations are included, especially J_2 (one of the largest perturbations for low Earth orbit), inclination and eccentricity are constantly changing. The iterative method does not exhibit that error, as shown in Figure 7.4, because it uses the same propagator as STK used to determine the true orbit, and therefore includes the orbital element change throughout the maneuver.
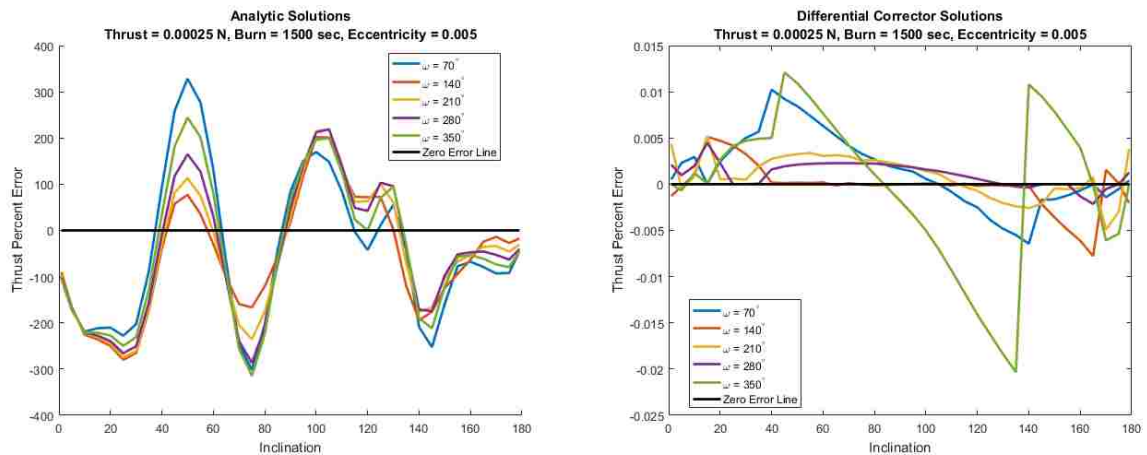

(a) Low Eccentric Orbit

(b) High Eccentric Orbit

Figure 7.4. J$_2$ Dynamics: Argument of Perigee vs Inclination

7.1.2.3. High-Precision orbit propagator. The error for both the low and high eccentric orbits are large for the low thrust maneuver using the analytic method. This error originates from the low fidelity of the thrust determination equation; it is attempting to determine a low fidelity thrust from high fidelity dynamics.

(a) Low Eccentric Orbit
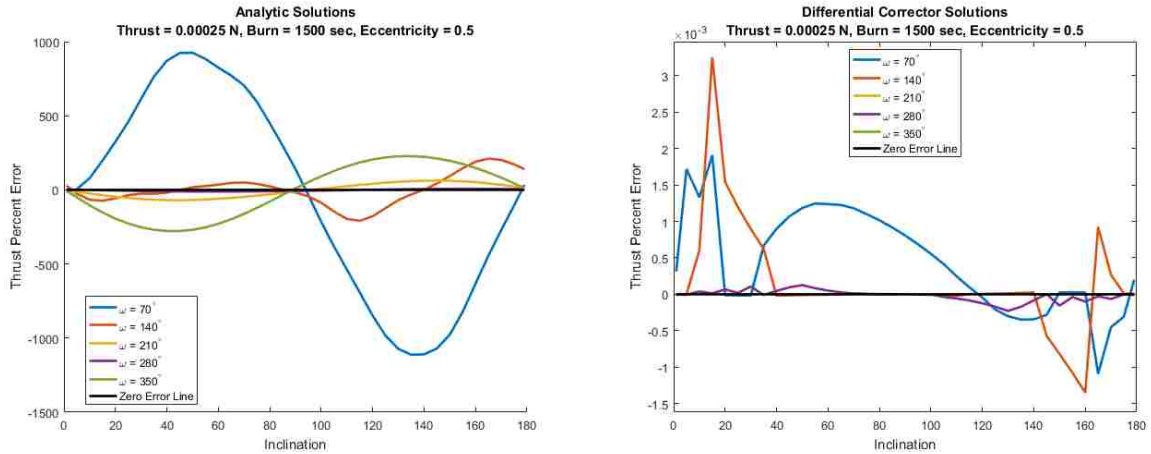
(b) High Eccentric Orbit

Figure 7.5. HPOP Dynamics: Argument of Perigee vs Inclination

The numeric method performed similarly to the Two-Body and J_2 dynamic solutions, remaining within $\pm 0.02\%$, as shown in Figure 7.5. When given the uncorrupted measurements, the numeric solution is very accurate, and the initial guess seems to make little difference. Multiple initial thrust vectors were used and the method always converged on the correct thrust magnitude and direction, though the number of iterations required to converge was increased when the initial guess was farther from the truth.

7.1.3. Summary. The numeric thrust determination method consistently out performed the analytic method and converged approximately to the true applied thrust for every low eccentricity orbit. The method does have some difficulty converging with higher eccentricity orbits consistently for the large initial thrust guess inaccuracy. This could be mitigated with a more accurate initial thrust estimate.

7.2. RESULTS WITH MEASUREMENT UNCERTAINTY

Now that the accuracy of the methods using the uncorrupted measurements are known, the methods are tested with a more realistic simulation. Uncertainty is added to the position and velocity measurements at the beginning ($\boldsymbol{x}_0$) and end ($\boldsymbol{x}_f$) of the maneuver

with RMS standard deviations of

$$\sigma_{x,rms} = 1.5 \text{ m} \qquad\qquad \sigma_{v,rms} = 10 \text{ mm/s}$$

Assuming that the position and velocity components have equal uncertainty, then the component position and velocity standard deviations are

$$\sigma_{x,rms} = \sqrt{\sigma_x^2 + \sigma_y^2 + \sigma_z^2}$$
$$\Rightarrow \sigma_x = \sigma_y = \sigma_z = \frac{\sigma_{x,rms}}{\sqrt{3}} = 0.866 \text{ m}$$

$$\sigma_{v,rms} = \sqrt{\sigma_v^2 + \sigma_v^2 + \sigma_v^2}$$
$$\Rightarrow \sigma_{\dot{x}} = \sigma_{\dot{y}} = \sigma_{\dot{z}} = \frac{\sigma_{v,rms}}{\sqrt{3}} = 5.774 \text{ mm/s}$$

The thrust determination algorithms are then run using these uncertain measurements instead of the truth. The thrust guess uses offset angles of $\alpha = 10°$ and $\beta = 75°$ from the truth and a thrust magnitude guess of 140% of the true magnitude. The true thrust is solely in the $\hat{h}$-direction, in accordance with a RAAN changing maneuver. Again, the analytic method assumed thrust was applied solely in the $\hat{h}$-direction with respect to the LVLH frame and the estimate state propagation was performed using the STK propagator that generated the true states. The thrust determination was performed using STK's HPOP dynamics for both chemical and electric modes for a range of orbits.

7.2.1. High Thrust (1 N). The analytic results with uncertainty follow the same general pattern as the results without uncertainty. The numeric results however are significantly higher. The thrust determination for the chemical propulsion is accurate to ±4% for both the high and low eccentric orbits, as shown in Figure 7.6.

7.2.2. Low Thrust (0.25 mN). The thrust determination for the electric propulsion was greatly affected by the measurement uncertainty, with a majority of the thrust errors in the ±60% range, shown in Figure 7.7. This could be due to the orbital element uncertainty
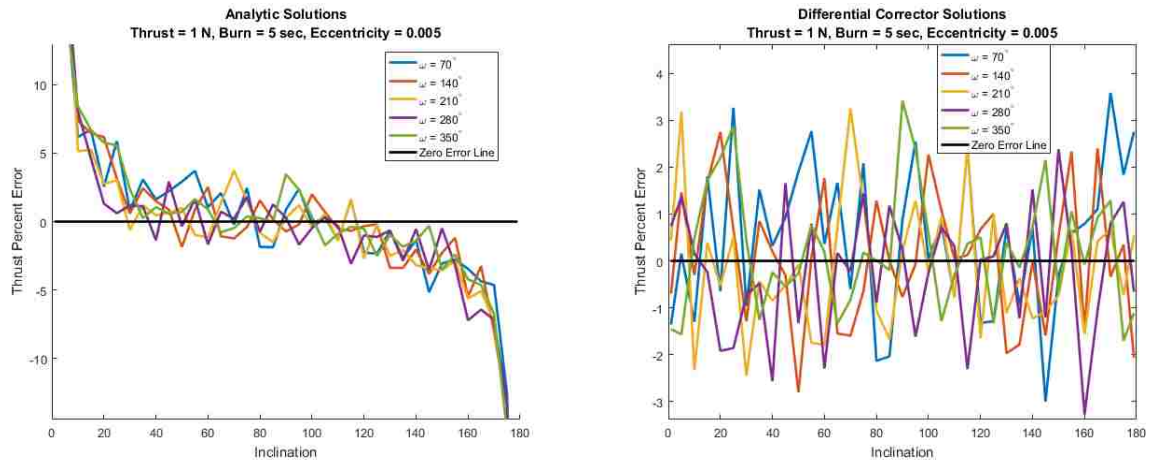
(a) Low Eccentric Orbit
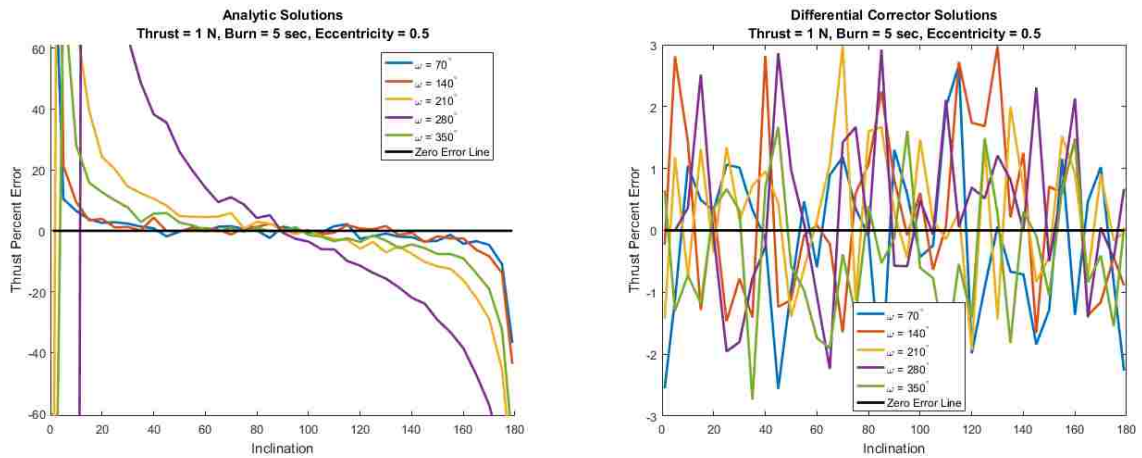
(b) High Eccentric Orbit

Figure 7.6. High Thrust: Argument of Perigee vs Inclination with Uncertainty

being on the same order as the element change from the maneuver. Another issue is the unfiltered measurements. The differential corrector determines the thrust that fits the initial and final orbital element measurements to some small tolerance, and therefore is determining the thrust vector between states that aren't the true states. This might be mitigated by applying a orbit determination filter to the corrupted measurements to better match the true states before implementing the numeric thrust determination algorithm.
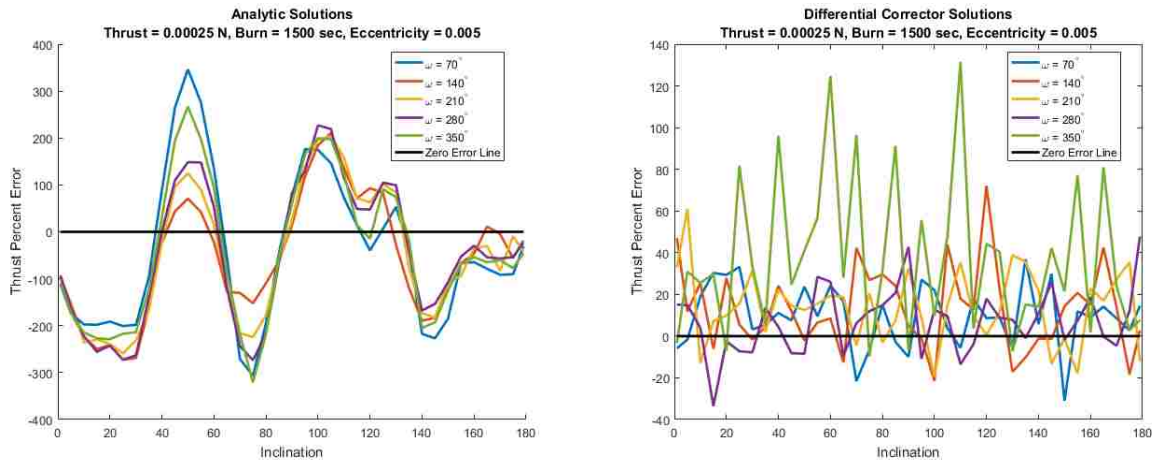
(a) Low Eccentric Orbit
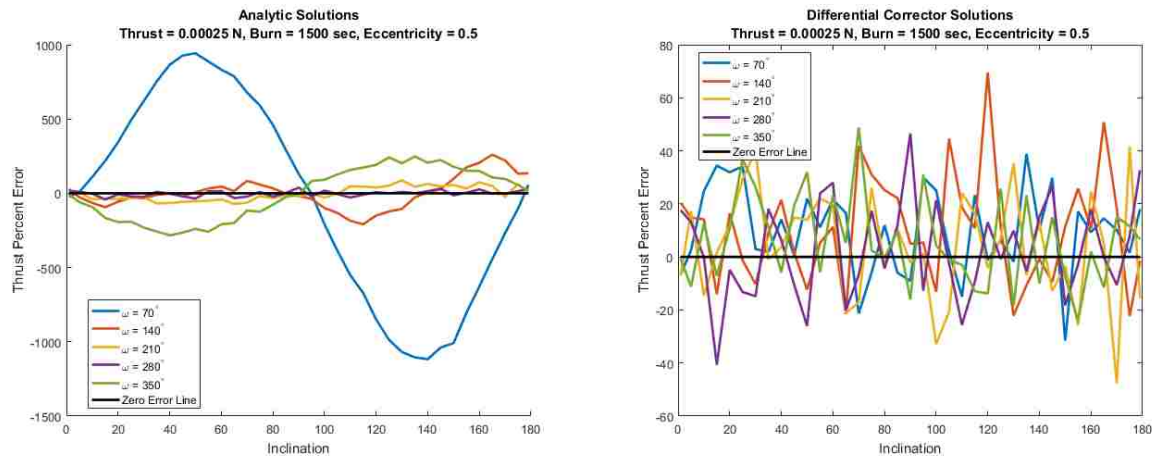
(b) High Eccentric Orbit

Figure 7.7. Low Thrust: Argument of Perigee vs Inclination with Uncertainty

7.2.3. Summary. The analytic thrust determination method with measurement corruption follows the same trend as the analytic without measurement noise as expected, because the same assumptions are used. The main source of error for the numeric thrust determination method is the convergence on the uncertain/incorrect measurement. This is expected and might be addressed by filtering the measurements before using the algorithm. The measurement uncertainty seems to affect higher eccentric orbits slightly less as well.

8. CONCLUSIONS

8.1. SUMMARY

Both the analytic and iterative methods in this research assume a constant thrust vector is applied with respect to the LVLH reference frame, but can be used with time-dependent thrust/force vectors. To do this with the analytic method would require multiple orbital element measurements during the maneuver because the method assumes a constant thrust/force vector between measurements. The differential corrector is designed to admit time varying thrust/force vectors already, but simplifies when the thrust vector is constant as shown in Section 4.

The analytic method provides a close approximation for low eccentricity orbits, particularly for propulsion systems with short finite maneuvers. The estimate would be a good initial guess for the differential corrector, especially if attitude knowledge was integrated into the analytic method.

The differential corrector is capable of determining an accurate estimate for low-thrust maneuvers given state measurements during a maneuver. The differential corrector is capable of determining the magnitude and direction of the external force acting on the satellite given accurate orbital element state measurements without requiring a "close" initial guess. The method does require more computational time with a guess that is further from the truth, but still converges to approximately the same result.

8.2. POSSIBLE APPLICATIONS

This research was conducted specifically for the APEX mission but can be adapted to other missions that require propulsive thrust/unknown force determination. With modification, this could even be used for orbit determination of maneuvering spacecraft. For

example, consider a satellite with an uncontrollable propellant leak; these methods could be used to determine how much thrust the malfunctioning satellite is producing to determine its orbit and possible future collisions with neighboring spacecraft. These methods could also passively determine the maneuvering capabilities of uncooperative spacecraft using line-of-sight orbit determination. Some propulsion system's efficiency will deteriorate over time, these methods could be used to determine the rate of deterioration as well.

8.3. FUTURE WORK

Some future works to be completed include: implementing a measurement filter to better fit maneuver trajectory before performing the thrust determination algorithm, incorporate attitude measurements into the algorithm, weighting the thrust correction based upon orbital element uncertainty, and convert the differential corrector into a batch least-squares to encompass multiple measurements. The end goal is to adapt this work into an orbit determination filter to more accurately represent maneuvering spacecraft on-orbit.

APPENDIX A

DERIVATION OF GAUSSIAN VARIATION OF PARAMETER EQUATIONS

With the help of the Vallado reference[6], (pages 630-636), the derivation of the Gaussian VOP equations start by defining the specific mechanical energy equation as

$$\xi = \frac{-\mu}{2a} \qquad \text{or} \qquad a = \frac{-\mu}{2\xi} \qquad (A.1)$$

where a and μ are the semimajor axis and the gravitational constant respectively. Allowing ξ to change with a specific perturbing force results in the time rate-of-change of energy from the work done by the perturbing force and the distance traveled as

$$\frac{d\xi}{dt} = \frac{\boldsymbol{F} \bullet \boldsymbol{V}}{m} = \dot{v}\left(\frac{dr}{dv}f_r + rf_\theta\right)$$

where $\boldsymbol{V}$, m, and v are the velocity of the satellite, mass of the satellite, and true anomaly of the orbit respectively. Taking the derivative of Equation A.1 with respect to time gives

$$\frac{da}{dt} = \frac{da}{d\xi}\frac{d\xi}{dt} = \frac{\mu}{2\xi^2}\frac{d\xi}{dt} \qquad (A.2)$$

Knowing that the angular momentum, h is defined as

$$h = r^2\dot{v} = \sqrt{\mu a(1 - e^2)} = \sqrt{\mu p}$$

it can be shown that

$$\dot{v} = \frac{h}{r^2}$$

and substituting into Equation A.2

$$\begin{aligned}
\frac{da}{dt} &= \frac{\mu \dot{v}}{2\xi^2} \left(\frac{re \sin(v)}{1 + e \cos(v)} f_r + r f_\theta \right) \\
&= \frac{2a^2 h}{\mu r} \left(\frac{e \sin(v)}{1 + e \cos(v)} f_r + f_\theta \right) \\
&= \frac{2a^2 p}{hr} \left(\frac{e \sin(v)}{1 + e \cos(v)} f_r + f_\theta \right) \\
&= \frac{2a^2}{h} \left(e \sin(v) f_r + \frac{p}{r} f_\theta \right)
\end{aligned}$$

To derive the remaining element variations the angular momentum rate-of-change is required and given by

$$\frac{d\boldsymbol{h}}{dt} = \boldsymbol{r} \times \boldsymbol{F} = \boldsymbol{r} \times \left(f_r \hat{\boldsymbol{R}} + f_\theta \hat{\boldsymbol{\Theta}} + f_h \hat{\boldsymbol{H}} \right) = r f_\theta \hat{\boldsymbol{H}} - r f_h \hat{\boldsymbol{\Theta}}$$

where $\hat{\boldsymbol{R}}$, $\hat{\boldsymbol{\Theta}}$, and $\hat{\boldsymbol{H}}$ represent the radial, velocity, and normal axis of the LVLH reference frame respectively. The angular momentum vector can also be differentiated in the LVLH system as

$$\frac{d\boldsymbol{h}}{dt} = \dot{h} \hat{\boldsymbol{H}}$$

therefore

$$\frac{d\boldsymbol{h}}{dt} = \dot{h} = r f_\theta$$

It is important to mention that $\dot{h} \neq d\boldsymbol{h}/dt$. Using the eccentricity equation

$$e = \sqrt{1 - \frac{p}{a}} = \sqrt{1 - \frac{h^2}{\mu a}}$$

and differentiating gives

$$\frac{de}{dt} = \frac{1}{2e}\left[\frac{-2h}{\mu a}\frac{dh}{dt} + \frac{h^2}{\mu a^2}\frac{da}{dt}\right] = \frac{-h}{\mu ae}\frac{dh}{dt} + \frac{h^2}{2\mu a^2 e}\frac{da}{dt}$$

$$= \frac{-h}{\mu ae}\left[r f_\theta\right] + \frac{h^2}{2\mu a^2 e}\left[\frac{2a^2 h}{\mu r}\left(\frac{e \sin(v)}{1 + e \cos(v)}f_r + f_\theta\right)\right]$$

$$= \frac{-hr}{\mu ae}f_\theta + \frac{h^3}{\mu^2 er}\left(\frac{e \sin(v)}{1 + e \cos(v)}f_r + f_\theta\right)$$

$$= \frac{h^3 e \sin(v)}{\mu^2 er(1 + e \cos(v))}f_r + \frac{h^3}{\mu^2 er}f_\theta - \frac{hr}{\mu ae}f_\theta$$

$$= \frac{\mu a(1 - e^2)h \sin(v)}{\mu^2 r(1 + e \cos(v))}f_r + \frac{h}{\mu e}\left(\frac{\mu a(1 - e^2)}{\mu r} - \frac{r}{a}\right)f_\theta$$

$$= \frac{rh \sin(v)}{\mu r}f_r + \frac{h}{\mu ae}\left(\frac{a^2(1 - e^2)}{r} - r\right)f_\theta$$

$$= \frac{h}{\mu}\left[\sin(v)f_r + \left(\cos(v) + \frac{e + \cos(v)}{1 + e \cos(v)}\right)f_\theta\right]$$

$$= \frac{p}{h}\left[\sin(v)f_r + \left(\cos(v) + \frac{e + \cos(v)}{1 + e \cos(v)}\right)f_\theta\right]$$

$$= \frac{1}{h}\left[p \sin(v)f_r + \left((p + r)\cos(v) + re\right)f_\theta\right]$$

The orbit inclination is found using

$$\cos(i) = \frac{\boldsymbol{h} \bullet \hat{\boldsymbol{K}}}{h}$$

Differentiating with respect to time gives

$$-\sin(i)\frac{di}{dt} = \frac{h\left(\frac{d\boldsymbol{h}}{dt} \bullet \hat{\boldsymbol{K}}\right) - \left(\boldsymbol{h} \bullet \hat{\boldsymbol{K}}\right)\frac{dh}{dt}}{h^2}$$

$$= \frac{h\left(r f_\theta \hat{\boldsymbol{h}} - r f_h \hat{\boldsymbol{\theta}}\right) \bullet \hat{\boldsymbol{K}} - h \cos(i)r f_\theta}{h^2}$$

$$= \frac{-r f_h \sin(i)\cos(\theta)}{h}$$

$$\frac{di}{dt} = \frac{r \cos(\theta)}{h}f_h$$

The right ascension of the ascending node (RAAN) is defined by

$$\cos\left(\Omega\right) = \frac{\hat{I} \bullet \left(\hat{K} \times h\right)}{\left|\hat{K} \times h\right|}$$

and differentiating gives

$$
\begin{aligned}
-\sin\left(\Omega\right)\frac{d\Omega}{dt} &= \frac{\hat{I} \bullet \left(\hat{K} \times \frac{dh}{dt}\right)\left|\hat{K} \times h\right| - \hat{I} \bullet \left(\hat{K} \times h\right)\frac{d}{dt}\left|\hat{K} \times h\right|}{\left|\hat{K} \times h\right|^2} \\
&= \frac{\hat{I} \bullet \left[\hat{K} \times \left(r f_\theta \hat{h} - r f_h \hat{\theta}\right)\right] h \sin\left(i\right)}{h^2 \sin^2\left(i\right)} - \ldots \\
&\qquad \ldots - \frac{h \cos\left(\Omega\right)\sin\left(i\right)\left(\frac{dh}{dt}\sin\left(i\right) + h\cos\left(i\right)\frac{di}{dt}\right)}{h^2 \sin^2\left(i\right)}
\end{aligned}
$$

where

$$\hat{I} \bullet \hat{K} \times \hat{H} = \cos\left(\Omega\right)\sin\left(i\right)$$

$$\hat{I} \bullet \hat{K} \times \hat{\Theta} = \hat{I} \times \hat{K} \bullet \hat{\Theta} = \sin\left(\Omega\right)\sin\left(\theta\right) - \cos\left(\Omega\right)\cos\left(\theta\right)\cos\left(i\right)$$

RAAN rate of change is then determined to be

$$\frac{d\Omega}{dt} = \frac{r\sin\left(\theta\right)}{h\sin\left(i\right)}f_h$$

Using a different form of the Orbital Equation and differentiating gives

$$r(1 + e\cos\left(v\right)) = \frac{h^2}{\mu}$$

$$r\left(\frac{de}{dt}\cos\left(v\right) - e\sin\left(v\right)\frac{dv}{dt}\right) = \frac{2h}{\mu}\frac{dh}{dt}$$

rearranging gives

$$\frac{dv}{dt} = \frac{\cot(v)}{e}\left[\frac{h}{\mu}\sin(v)f_r + \frac{h}{\mu ae}\left(\frac{a^2(1-e^2)}{r} - r\right)f_\theta\right] - \frac{2h}{\mu e\sin(v)}f_\theta$$

$$= \frac{h}{\mu e}\cos(v)f_r - \frac{h(2 + e\cos(v))\sin(v)}{\mu e(1 + e\cos(v))}f_\theta$$

$$= \frac{p}{he}\cos(v)f_r - \frac{p(2 + e\cos(v))\sin(v)}{he(1 + e\cos(v))}f_\theta$$

$$= \frac{1}{he}\left(p\cos(v)f_r - \frac{[p + p(1 + e\cos(v))]\sin(v)}{1 + e\cos(v)}f_\theta\right)$$

$$= \frac{1}{he}\left(p\cos(v)f_r - (r + p)\sin(v)f_\theta\right)$$

The two-body rate (h/r^2) is then added to obtain the actual true anomaly rate as

$$\frac{dv}{dt} = \frac{h}{r^2} + \frac{1}{he}\left(p\cos(v)f_r - (r + p)\sin(v)f_\theta\right)$$

The last orbital element rate of change to determine is the argument of periapsis. Recalling that the argument of latitude $(\theta = v + \omega)$ gives

$$r\cos(v + \omega) = \frac{(\hat{K} \times h)\bullet r}{|\hat{K} \times h|}$$

Differentiating results in

$$-r\sin(\theta)\left(\frac{d\omega}{dt} + \frac{dv}{dt}\right) = \frac{|\hat{K} \times h|\left(\hat{K} \times \frac{dh}{dt}\bullet r\right) - (\hat{K} \times h\bullet r)\frac{d}{dt}|\hat{K} \times h|}{|\hat{K} \times h|^2}$$

Rearranging gives

$$\frac{d\omega}{dt} = \frac{-|\hat{K} \times h|\left(\hat{K} \times \frac{dh}{dt}\bullet r\right) + (\hat{K} \times h\bullet r)\frac{d}{dt}|\hat{K} \times h| - \frac{dv}{dt}|\hat{K} \times h|^2 r\sin(\theta)}{|\hat{K} \times h|^2 r\sin(\theta)}$$

where

$$\hat{K} \times \hat{H} \bullet r = r \sin{(i)} \cos{(\theta)}$$

$$\hat{K} \times \hat{\Theta} \bullet r = -r \cos{(i)}$$

$$\hat{K} \times h \bullet r = rh \sin{(i)} \cos{(\theta)}$$

substituting dv/dt and dh/dt the argument of periapsis rate of change is then

$$\frac{d\omega}{dt} = \frac{1}{he} \left(-p \cos{(v)} f_r + (r + p) \sin{(v)} f_\theta \right) - \frac{r \cot{(i)} \sin{(\theta)}}{h} f_h$$

The argument of latitude rate can also be found as

$$\frac{d\theta}{dt} = \frac{dv}{dt} + \frac{d\omega}{dt}$$

Summarizing:

$$\frac{da}{dt} = \frac{2a^2 h}{\mu r} \left(\frac{e \sin{(v)}}{1 + e \cos{(v)}} f_r + f_\theta \right) \tag{A.3}$$

$$\frac{de}{dt} = \frac{1}{h} \left[p \sin{(v)} f_r + \left((p + r) \cos{(v)} + re \right) f_\theta \right] \tag{A.4}$$

$$\frac{di}{dt} = \frac{r \cos{(\theta)}}{h} f_h \tag{A.5}$$

$$\frac{d\Omega}{dt} = \frac{r \sin{(\theta)}}{h \sin{(i)}} f_h \tag{A.6}$$

$$\frac{d\omega}{dt} = \frac{1}{he} \left(-p \cos{(v)} f_r + (r + p) \sin{(v)} f_\theta \right) - \frac{r \cot{(i)} \sin{(\theta)}}{h} f_h \tag{A.7}$$

$$\frac{dv}{dt} = \frac{h}{r^2} + \frac{1}{he} \left(p \cos{(v)} f_r - (r + p) \sin{(v)} f_\theta \right) \tag{A.8}$$

$$\frac{d\theta}{dt} = \frac{h}{r^2} - \frac{r \cot{(i)} \sin{(\theta)}}{h} f_h \tag{A.9}$$

where

$$r = \frac{a(1 - e^2)}{1 + e \cos{(v)}}$$

APPENDIX B

LEGENDRE POLYNOMIALS

The Legendre polynomials for the function, $P_{l,m}\left[\sin\left(\phi_{gc}\right)\right]$ for the first four zonal harmonics are given as[6]

$P_{0,0} = 1$

$P_{1,0} = \sin\left(\phi_{gc}\right)$

$P_{1,1} = \cos\left(\phi_{gc}\right)$

$P_{2,0} = \dfrac{1}{2}\left(3\sin^2\left(\phi_{gc}\right) - 1\right)$

$P_{2,1} = 3\sin\left(\phi_{gc}\right)\cos\left(\phi_{gc}\right)$

$P_{2,2} = 3\cos^2\left(\phi_{gc}\right)$

$P_{3,0} = \dfrac{1}{2}\left(5\sin^3\left(\phi_{gc}\right) - 3\sin\left(\phi_{gc}\right)\right)$

$P_{3,1} = \dfrac{1}{2}\cos\left(\phi_{gc}\right)\left(15\sin^2\left(\phi_{gc}\right) - 3\right)$

$P_{3,2} = 15\cos^2\left(\phi_{gc}\right)\sin\left(\phi_{gc}\right)$

$P_{3,3} = 15\cos^3\left(\phi_{gc}\right)$

$P_{4,0} = \dfrac{1}{8}\left(35\sin^4\left(\phi_{gc}\right) - 30\sin^2\left(\phi_{gc}\right) + 3\right)$

$P_{4,1} = \dfrac{5}{2}\cos\left(\phi_{gc}\right)\left(7\sin^3\left(\phi_{gc}\right) - 3\sin\left(\phi_{gc}\right)\right)$

$P_{4,2} = \dfrac{15}{2}\cos^2\left(\phi_{gc}\right)\left(7\sin^2\left(\phi_{gc}\right) - 1\right)$

$P_{4,3} = 105\cos^3\left(\phi_{gc}\right)\sin\left(\phi_{gc}\right)$

$P_{4,4} = 105\cos^4\left(\phi_{gc}\right)$

REFERENCES

[1] Berg, S. P. and Rovey, J. L., "Assessment of Multimode Spacecraft Micropropulsion Systems," *Journal of Spacecraft and Rockets*, 2017, **54**, pp. 592–601.

[2] Myers, R. M., Oleson, S. R., Curran, F. M., and Schneider, S. J., "Small Satellite Propulsion Options," 30th Joint Propulsion Conference, June 1994 .

[3] Zona, K., "Ion Propulsion: Farther, Faster, Cheaper," NASA Glenn Research Center, 2004.

[4] Kelecy, T. and Jah, M., "Detection and Orbit Determination of a Satellite Executing Low Thrust Maneuvers," *Acta Astronautica*, 2010, **66**, pp. 798–809.

[5] Morton, B. and Withrow-Maser, S., "On-Orbit CubeSat Performance Validation of a Multi-Mode Micropropulsion System," *Proceedings of the AIAA/USU Conference on Small Satellites, Frank J. Redd Student Scholarship Competition*, 2017, (SS17-VIII-4).

[6] Vallado, D. A. and McClain, W. D., *Fundamentals of Astrodynamics and Applications*, Space Technology Library, Microcosm Press, 2013, ISBN 9781881883180.

[7] Barrodale, I., Powell, M. J. D., and Roberts, F. D. K., "The Differential Correction Algorithm for Rational ℓ_∞-Approximation," *SIAM Journal on Numerical Analysis*, 1972, **9**, pp. 493–504.

[8] Escobal, P. R., *Methods of Orbit Determination*, R. E. Krieger Publishing Company, 1976, ISBN 9780882753195.

[9] Decell, H. P., "An application of generalized matrix inversion to sequential least squares parameter estimation," National Aeronautics and Space Administration (NASA), 1965.

[10] "Space vehicle accelerometer applications," National Aeronautics and Space Administration (NASA), 1972.

[11] Seiko Epson Corporation, "IMU:M-G364 - Sensing System - Epson," `https://global.epson.com/products_and_drivers/sensing_system/imu/g364/`, Online; accessed 23 September 2016.

VITA

Bradyn William Morton was born in 1993 in Kirksville, MO. In August 2011 he began his collegiate career at the Missouri University of Science and Technology. He graduated Cum Laude with two Bachelors of Science degrees in Aerospace and Mechanical Engineering in May 2016. Bradyn started graduate school August 2016 at the Missouri University of Science and Technology. In July 2018 he received his Masters of Science degree in Aerospace Engineering from the Missouri University of Science and Technology.